SOLITON PULSE GENERATION FOR DENSE WAVELENGTH DIVISION MULTIPLEXING ENHANCEMENT

NARONG SANGWARA

A THESIS SUBMITTED IN PARTIAL FULFILLMENT

OF THE REQUIREMENT FOR THE DEGREE OF

DOCTOR OF PHILOSOPHY IN APPLIED PHYSICS

FACUTY OF SCIENCE

KING MONGKUT'S INSTITUTE OF TECHNOLOGY LADKRABANG

2009

KMITL-2009-SC-D-030-044

หัวข้อวิทยานิพนธ์	การสร้างพัลส์โซลิตอนสำหรับการผสมสัญญาณตามความยาวคลื่นแบบความหนาแน่นสูง
นักศึกษา	นาย ณรงค์ สังวาระ
รหัสประจำตัว	51067003
ปริญญา	ปรัญญาดุษฎีบัณฑิต
สาขาวิชา	ฟิสิกส์ประยุกต์
พ.ศ.	2552
อาจารย์ผู้ควบคุมวิทยานิพนธ์	รศ.ดร.ปรีชา ยุพาพิน

บทคัดย่อ

งานวิจัยนี้เป็นการนำเสนอการสร้างพัลส์โซลิตอนที่เดินทางผ่านเข้าไปในวงแหวนสั่นพ้อง ระบบประกอบด้วยวงแหวนสั่นพ้องขนาดเล็กสองวงและตัวมัลติเพล็กซ์ของแอดดรอป ซึ่งสามารถนำมาต่อรวมกันเป็นระบบเดียว สัญญาณช่วงความถี่ของคลื่นที่กว้างนั่นสามารถสร้างโดยการแพร่พัลส์โซลิตอนในความไม่เป็นเชิงเส้นของเคอร์ การปรับพัลส์โซลิตอนที่โหมดคงที่และโหมดที่ขึ้นกับเวลาทำได้โดยการใช้ตัวมัลติเพล็กซ์ของแอดดรอป ผลที่ได้รับแสดงการสามารถสร้างพัลส์โซลิตอนจำนวนมากภายในวงแหวนสั่นพ้องขนาดเล็กเป็นผลสำเร็จ สิ่งที่ใช้เป็นประโยชน์สำหรับการสื่อสารระยะไกล คือการผสมสัญญาณตามความยาวคลื่นแบบความหนาแน่นสูงซึ่งมีความสำคัญมากในเรื่องเพิ่มจำนวนช่องและช่องว่างของสัญญาณ จะได้ช่วงปลอดสเปคตรัมกว้างถึง 600 พิโกเมตร

Thesis Title	Soliton Pulse Generation for Dense Wavelength Division Multiplexing Enhancement
Student	Narong Sangwara
Student ID	51067003
Degree	Doctor of Philosophy
Programme	Applied Physics
Year	2009
Thesis Advisor	Assoc. Prof. Dr. Preecha Yupapin

ABSTRACT

This thesis presents an optical system that can be used to form the multi soliton pulses within the micro ring resonators. The system consists of two micro ring resonators and an add/drop multiplexer that can be integrated into a single system. The large bandwidth signal is generated by using a soliton pulse propagating in a Kerr type nonlinear medium. The tuned soliton pulses in either spatial or temporal modes are obtained by using the add/drop multiplexer. Results obtained have shown that the multi soliton pulses can be localized coherently within the micro ring waveguide. This is shown that the generation of the multi soliton pulses within the micro ring resonator is achieved, which is available for long distance communication with dense wavelength division multiplexing (DWDM). The significant increasing in channel number and spacing are obtained, whereas the large free spectrum range (FSR) of 600 pm is achieved.

ACKNOWLEDGEMENTS

While I have worked on this thesis for over three years, several people have contributed to this effort directly and indirectly. I would like to express my thankfulness to all of them.

No student thesis is achievable without the guidance and assistance of the thesis advisor. I was fortunate to have Assoc. Prof. Dr. Preecha Yupapin as my thesis advisor. His patient guidance, encouragement and enthusiasm throughout the development of my thesis were highly prized.

I would like to extend my appreciation to Asst. Prof. Suchit Srichai and Mr.Suchrat Heng and Mr.Boonkum kongmaha Senior Lecturer, the Department of Physics, Faculty of Science and Technolog, Rajamangala University of Technology Krungthep, for their support and advice.

My profound gratitude must go to my parents for infinite encouraging and understanding me. They have always been there for me with this thesis. With their love, my thesis has been possible. Special thanks are due to my best friends (ARCP) for their support. Some of them shared my insanity of doing a doctoral degree.

I would like to sincerely thank to the Department of Applied Physics, Faculty of Science, King Mongkut's Institute of Technology Landkrabang for offering this academic opportunity to me. I am extremely grateful to Rajamangala University of Technology Krungthep for awarding me the scholarship.

Narong Sangwara

TABLE OF CONTENTS

TABLE OF CONTENTS (CONTINUED)

LIST OF FIGURES

LIST OF FIGURES (CONTINUED)

LIST OF FIGURES (CONTINUED)

CHAPTER 1
INTRODUTION

1. Motivation

The use of light as communication methods can date back to antiquity if we define optical communications in a broader way . People had used mirrors, fire beacons, or smoke signals to convey a single piece of information. The modern fiber-optic communications started around 1970s when GaAs semiconductor laser was invented and the optical fiber loss could be reduced to 20 dB/km in the wavelength region near 1μm. Since then, fiber-optic communication has rapidly developed. The enormous progress of lightwave systems can be grouped into several generations. A widely used figure of merit is the bit rate-distance product, BL, where B is the bit rate and L is the repeater spacing. Figure. 1.1 shows the increase of bit rate-distance product over the developing of lightwave systems. These data are quantified through various laboratory experiments [1].

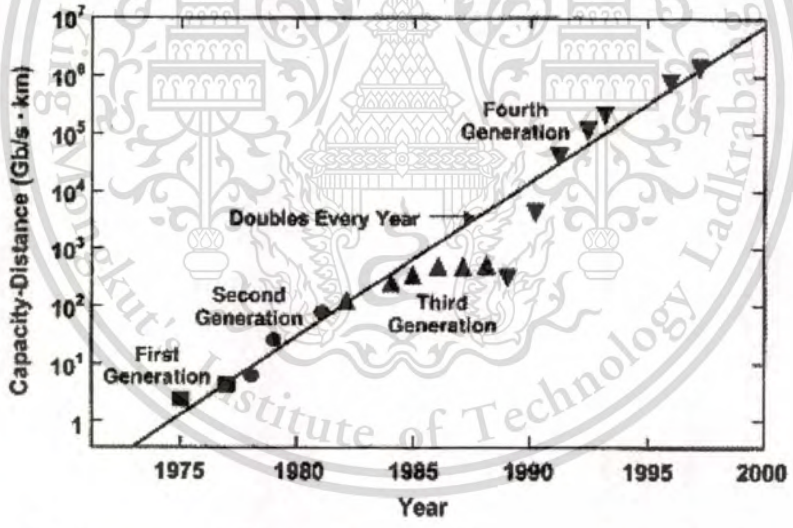

Figure. 1.1: Increase in BL product over the developing lightwave systems.

The first generation of light wave systems was commercially available in 1980. It operated near 800 nm and used GaAs semiconductor lasers. The data rate of the light wave systems could reach 45 Mb/s with repeater spacing up to 10 km.

The second generation of light wave systems became commercially available in late 1980s. It operated in the wavelength region near 1.3μm, where fiber loss is below 1 dB/km and optical fiber has exhibited minimum dispersion in this region. From the early 1980s, the developments of InGaAsP semiconductor lasers and detectors operating near 1.3μm and the use of single-mode fibers have contributed to

the availability of the second generation of light wave systems. By 1987, the second-generation light wave systems with data rate of 1.7 Gb/s and a repeater spacing of 50 km were available.

The third-generation light wave systems with data rate of 2.5 Gb/s became commercially available in 1990. It was known that silica fibers had the minimum loss (0.2-dB/km) near the wavelength 1.55μm. Unfortunately there is large fiber dispersion near 1.55μm. To overcome this problem, dispersion-shifted fiber and single-longitudinal-mode lasers were developed. Drawback of the third-generation light wave system was that the signal has to be electronically regenerated periodically with the repeater spacing of typically from 60 to 70 km.

Use of erbium-doped fiber amplifiers (EDFA) and wavelength-division multiplexing (WDM) is the distinct character of fourth-generation light wave system. EDFA was developed in 1985 and was commercially available in 1990. EDFA made it possible to transmit optical signals up to tens of thousands of kilometer without using electronic regenerator. The advent of WDM technique started a revolution and increased the capacity of light wave system enormously. By 1996, commercial transatlantic and transpacific cable systems became available. A demonstration of optical transmission over 11,300 km using actual submarine cables at a data rate of 5Gb/s [1] was realized in the same year. Since then, many submarine light wave systems have been developed worldwide.

The next generation of light wave system, the fifth-generation of light wave system has been under development for a while. The emphasis of research can be commonly categorized into two groups. One emphasis is to extend the wavelength range to L-band (1570nm – 1610nm) and S-band (1485nm – 1520nm) to increase the number of channels in WDM. Currently light wave systems are operating in the conventional wavelength window, known as C-band, which is from 1530 nm to 1565 nm. Another emphasis is to increase the data rate of each channel. Many experiments have been done operating at data rate of 10 Gb/s or 40 Gb/s since year 2000. In such higher datarate light wave systems, dispersion compensation management and combating of nonlinearity degrading effects like SPM, XPM and FWM are becoming urgent. In this issue, modulation formats has been a key factor.

Optical soliton has been recognized as a nonlinear solitary wave for years [2,3]. Since then, it has been widely investigated in several subjects such as in physics, mathematics and communication, especially, in optical communication. Generally, the common properties of a soliton known as self-phase modulation (SPM) and cross-phase modulation (XPM) are the challenged behaviors. Furthermore, the non-dispersion behavior of the soliton is the advantageous key. This can be used in long-haul communication, where the long-distance link without a repeater can be employed. The other interesting soliton behavior is the localization, where the soliton pulse can be trapped and stored within the periodic medium, which is useful in many areas of applications. Generally, the soliton pulse can be recovered, when the balance between dispersion and nonlinear lengths of the soliton pulse exhibits the soliton behavior known as self-phase modulation, which occurs when the matching between the soliton property and localized media occurred. When the generation of the localized soliton pulse is achieved, it is available for applications in many areas of research in science and technology. Recently, the use of a chaotic soliton to form a fast light generation within

a tiny device known as a micro-ring resonator (waveguide) has been reported by Yupapin et al. [4]. They have shown that the large bandwidth can be compressed coherently with a small group velocity. In practice, such devices have been fabricated and used [5–7] in various applications.

In this thesis, we show that the large bandwidth of soliton pulse is generated and filtered within the micro- ring resonator system. The selected (tuned) pulse is coherently localized and stored within the ring device. In applications, we can use the tuned soliton pulses to perform the required applications such as dense wavelength division multiplexing (DWDM)-based soliton communication, optical and quantum memory, and multi-soliton sources.

1.2 Objective

The objectives of the research are following

1.2.1 To study and understand the optical ring resonator.

1.2.2 To study and understand optical solitons.

1.2.3 To study optical solitons in nonlinear microring resonators.

1.2.4 To study soliton pulse generation for DWDM.

1.3 Scope of the Research

The soliton pulses within the micro ring resonators. The system consists of two micro ring resonators and an add/drop multiplexer that can be integrated into a single system. The large bandwidth signal is generated by using a soliton pulse propagating in a Kerr type nonlinear medium. The tuned soliton pulses in either spatial or temporal modes are obtained by using the add/drop multiplexer. The multi soliton pulses can be localized coherently within the micro ring waveguide. This is shown that the generation of the multi soliton pulses within the micro ring resonator is achieved, which is available for long distance communication with dense wavelength division multiplexing (DWDM).

1.4 Research Procedure and Schedule

Step for doing this research are summarized here.

1.4.1 Study basic knowledge related literature about optical ring resonator.

1.4.2 Study basic knowledge related literature about optical solitons.

1.4.3 Study optical solitons in nonlinear microring resonators

1.4.4 Implement each the dark-bright signal amplification using MATLAB programming.

1.4.5 Compare and contrast the result of soliton pulse generation in microring resonators for DWDM.

1.4.6 Conclude the work and write the documents.

CHAPTER 2
OPTICS RING RESONATOR

Optical ring resonators consist of a waveguide in a closed loop coupled to one or more input/output waveguides. When light of the appropriate wavelength is coupled to the loop by the input waveguide, it builds up in intensity over multiple round-trips due to constructive interference. It can then be picked up by a detector waveguide. Since only some wavelengths resonate in the loop, if function as a filter.

2.1. Ring Resonator

In this chapter, I will describe the theoretical background for this thesis. To begin, section 2.1.1 discuss the history of ring resonator and the material system which was used for the planar waveguide. Section 2.1.2 discusses the basic optical ring resonators and the used model using Z-transform. Section 2.1.3 discusses physical meaning of resonance characteristics of ring resonators. In the last section discusses the basic concept of optical add/drop filter.

2.1.1 Field Enhancement

At steady state, the field circulating inside the resonator can be also written as

$$E_{r1} = (1-\gamma)^{1/2} \times \left[j \cdot E_i \cdot \sqrt{\kappa} + E_{r1} \cdot \sqrt{1-\kappa} \cdot a \cdot z^{-1} \right]. \tag{2.1}$$

Therefore the ratio of the circulating field to the input field which does not take into account coupling losses ($\gamma = 0$) is given by

$$\frac{E_{r1}}{E_i} = \frac{j\sqrt{\kappa}}{1-\sqrt{(1-\kappa)} \cdot a \cdot z^{-1}}. \tag{2.2}$$

We define the Field Enhancement Factor FE, as the magnitude of the ratio of the circulating field inside the resonator E_{r1}, to the input field E_i, at resonance, i.e., $\phi = 0$. The FE is thus given by

$$FE = \left| \frac{E_{r1}}{E_i} \right|_{\phi=0} = \frac{\sqrt{\kappa}}{1-\sqrt{(1-\kappa)} \cdot a}. \tag{2.3}$$

The higher the FE, the higher the built up intensity inside the resonator and thus the lower the amount of input power required to induce nonlinear effects. Therefore, it is very important to understand what factors limit the FE for a given ring resonator. In Figure. 2.1, we plot Eq. (2.3), for different values of the round trip field transmission, a, and field coupling coefficient, κ. As can be seen, the higher the value of a and therefore the lower the round trip loss, the higher the FE obtained by the resonator. Also, for a given value of a, the FE peaks at a maximum then decreases as a function of κ, as we will discuss in the following subsection.

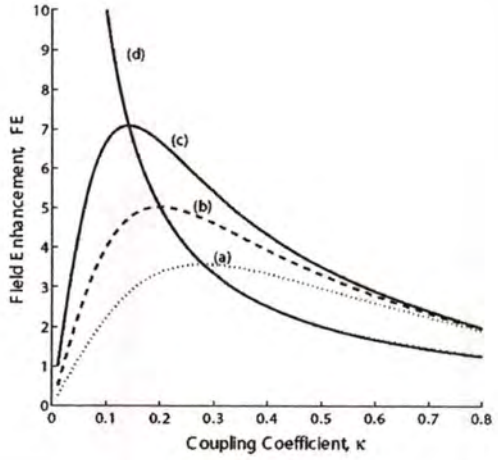

Figure 2.1: Field Enhancement, FE, versus the coupling coefficient κ, for: (a) $a = 0.96$, (b) $a = 0.98$, (c) $a = 0.99$, and (d) $a = \sqrt{1-\kappa}$

2.1.2 Critical Coupling

The maximum FE that is feasible by a ring resonator can be obtained mathematically by differentiating Eq. (2.3) with respect to κ, and equating the result to 0. Doing the math, we find that this happens when $a = \sqrt{1-\kappa}$, and it yields a maximum FE equal to $1/\kappa$. Moreover, at resonance, the transmission-transfer function, given by Eq. (2.1), has a magnitude of 0, when the above condition is met. That is all the power coupled to the resonator is equal to the power consumed by or lost inside the resonator. This criterion is known as critical coupling and is desirable in some applications where high switching contrast is required. In Figure. 2.2, we plot the throughput transmission and the normalized resonating intensity for a critically coupled ring resonator. At resonance, a complete extinction is achieved for the throughput transmitted intensity. On the other hand, the circulating intensity inside the ring is much higher than the input intensity due to the FE effect.

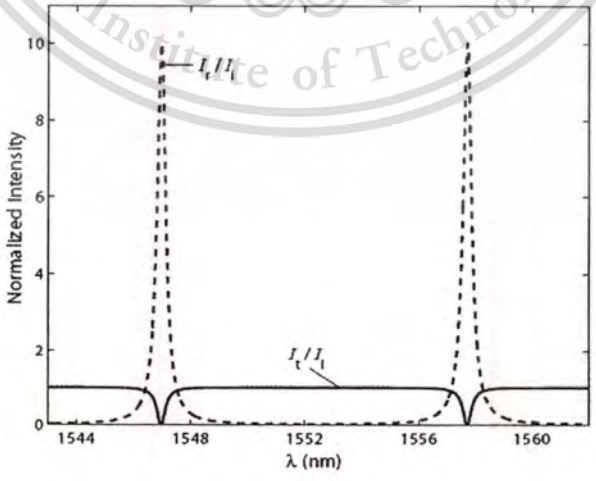

Figure 2.2: Throughput intensity transmission (solid line) and normalized resonating intensity (dashed line) for a critically coupled ring resonator that has a refractive index of 3.4, diameter of 20 μm, and a power coupling coefficient $\kappa^2 = 10\%$.

2.1.3 Resonator Bandwidth

The resonance bandwidth determines how fast optical data can be processed by a ring resonator. The resonator bandwidth is given by the full width at half maximum (FWHM) of the ring intensity resonance or its 3 dB bandwidth ($\frac{I_t}{I_i}(\phi) = 0.5$). It also is a measure of a sharpness of the resonance. The FWHM of the single ring resonator is given by

$$\delta\phi = \frac{2 \cdot (1 - x \cdot y)}{\sqrt{x \cdot y}}. \tag{2.4}$$

To understand how the bandwidth of the resonator is affected by the coupling coefficient, κ we will consider a critically coupled ring resonator. In such a case, Eq. (2.4) results in

$$\delta\phi = \frac{2 \cdot \kappa}{\sqrt{1 - \kappa}}. \tag{2.5}$$

Therefore, the lower the coupling coefficient, κ the smaller the resonance bandwidth. On the other hand, Eq. (2.5) shows that the lower the coupling coefficient, κ the higher the FE of the resonator.

2.1.4 Resonator Finesse

The finesse F of the resonator is defined as the ratio of the free spectral range and the full width at half maximum of a resonance. For the Figure. 2.3 using FSR in term of phase is equal to 2π and thus the finesse is given by

$$F = \frac{2\pi}{\delta\phi} = \frac{\pi \cdot \sqrt{x \cdot y}}{(1 - x \cdot y)}. \tag{2.6}$$

The finesse gives the resoling power of the resonator when used as a transmission filter. An interesting fact is that resonator finesse is independent on its dimension or circulating light wavelength. It is only a function of coupling coefficient and internal loss. The finesse of a critical coupling ($x = y$) is given by

$$F_{x=y} = \frac{\pi \cdot y}{1 - y^2} = \frac{\pi \cdot \sqrt{1 - \kappa}}{\kappa}. \tag{2.7}$$

$$F_{x=y} = \frac{\pi \cdot x}{1 - x^2} = \frac{\pi \cdot D \exp^{-\alpha L/2}}{1 - D^2 \exp^{-\alpha L}}. \tag{2.8}$$

The finesse F depending on the coupling coefficient κ at the point of maximum on-off ratio is shown in Figure. 2.3.

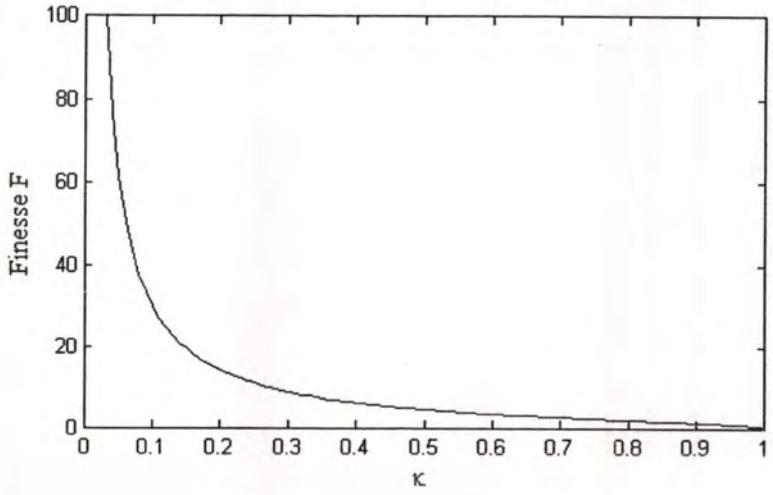

Figure 2.3: Finesse depending on the coupling coefficient κ at the point of maximum on-off ratio.

The finesse depending on the intensity attenuation coefficient of the ring α at the point of maximum on-off ratio for a ring resonator with $R = 100$ μm is shown in Figure. 3.8.

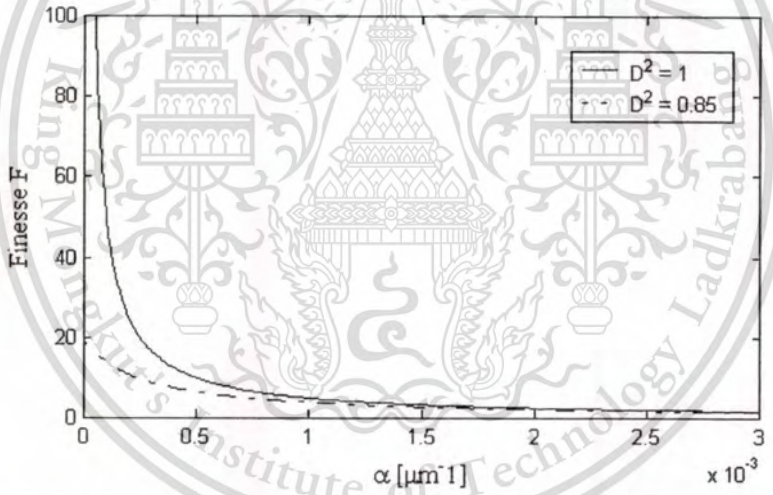

Figure 2.4: Finesse depending on α at the point of maximum on-off ratio. A high finesse F > 10 can be realized using a coupling coefficient $\kappa < 0.3$, a coupler with $\gamma < 15\%$ and an intensity attenuation coefficient of the ring $\alpha < 0.0001\,\mu m^{-1}$.

2.1.5 Free Spectal Range, FSR

The frequency spacing between two resonance peaks is call the free spectral range which is calculated as follows: The phase constant which corresponds to $\phi = 2.m.\pi$ is defined as k. The phase constant which corresponds to $\phi = 2.(m+1).\pi$ is defined as $k+\Delta k$. The frequency shift Δf and the wavelength shift $\Delta\lambda$ are related to variation of the phase constant Δk as $\Delta f = \frac{c}{2\pi}.\Delta k$ and $\Delta\lambda = -(\frac{\lambda^2}{2\pi}).\Delta k$. The resonance spacing in terms of the frequency f and the wavelength λ are given by

$$\Delta f = \frac{c}{n_{gr}.L}, \tag{2.9}$$

$$\Delta\lambda = \left| -\frac{\lambda^2}{n_{gr}.L} \right|, \tag{2.10}$$

where n_{gr} is the group refractive index, which is defined as

$$n_{gr} \equiv n_{eff} - \lambda \frac{dn_{eff}}{d\lambda}. \tag{2.11}$$

Using $\delta\phi = \delta(k_n.L) = \frac{2\pi}{F}$, the FWHM $\delta\phi$ in term of frequency and wavelength at the resonance peaks are given by

$$\delta f = \frac{c}{F.n_{gr}.L}. \tag{2.12}$$

$$\delta f = \frac{\lambda^2}{F.n_{gr}.L}. \tag{2.13}$$

The finesse can also be calculated using the FSR (Δf or $\Delta\lambda$) and the FWHM (δf or $\delta\lambda$) of a filter and is given by

in the frequency domain:
$$\frac{\Delta f}{\delta f} = \frac{\frac{c}{n_{gr}.L}}{\frac{c}{F.n_{gr}.L}} = F. \tag{2.14}$$

in the wavelength domain:
$$\frac{\Delta\lambda}{\delta\lambda} = \frac{\frac{\lambda^2}{n_{gr}.L}}{\frac{\lambda}{F.n_{gr}.L}} = F. \tag{2.15}$$

2.16 Quality Factor

Another value for characterization of ring resonators is the quality factor Q. The Q factor of a resonator is a measure of the sharpness of the resonance. In analogy with electrical circuits, the quality factor of an optical waveguide due its stored energy and the power lost per optical cycle. The Q is defined as

$$Q = \omega \frac{store\ energy}{power\ loss}, \tag{2.16}$$

where ω is the frequency of light coupled to the resonator. The Q factor of the resonator can be calculated from

$$Q = \frac{f_o}{\delta f} = \frac{\lambda_0}{\delta \lambda}. \tag{2.17}$$

The Q factor is the ratio of the absolute frequency f_0 or absolute wavelength λ_0 to the 3 dB bandwidth (δf or $\delta \lambda$). The shape and the bandwidth (δf or $\delta \lambda$) of the filter response is determined by the Q factor.

The finesse and the Q factor are both important when one is interested in both the FSR (Δf or $\Delta \lambda$) and the 3 dB bandwidth (δf or $\delta \lambda$). They are related by

$$\frac{Q}{F} = \frac{f_0}{F} = \frac{\lambda_0}{\Delta \lambda}. \tag{2.18}$$

The Q factor depending on the finesse F for a ring resonator with a radius $R = 100\ \mu m$, $50\ \mu m$ and $10\ \mu m$, a group refractive index $n_{gr} = 3.44$ at the wavelength of $\lambda = 1.55\ \mu m$ is shown in Figure. 2.5.

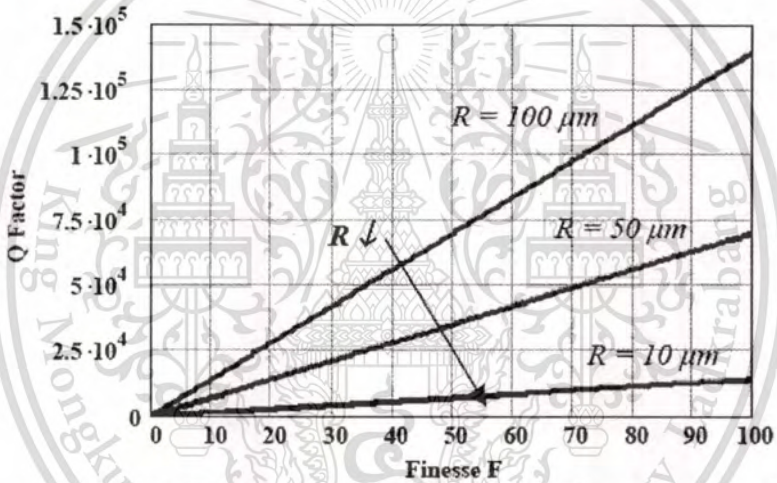

Figure 2.5: Q factor depending on the finesse F for a specific radius R.

A high finesse (>100) and a low Q factor (<2.5x104) is obtained, for example, for ring resonators with a low radius ($R < 20\ \mu m$). A ring resonator for a given specific bandwidth (δf or $\delta \lambda$) can be designed using the following steps

$$\delta f \text{ or } \delta \lambda \xrightarrow{Eq.3.28} Q \xrightarrow{Eq.3.29} F, F \xrightarrow{Eq.3.18, Eq.3.19} \kappa, \alpha \text{ (point of maximum on-off ratio)}$$

High Q cavities can serve for example as building blocks for optical signal processing applications or for laser applications where high quality factors are required. The basic figures for the description of a single ring resonator with one input waveguide have been presented. This model is extended to multiple coupled ring resonators in the next chapters

2.2 All-Pass or Phase Filter

A key element for controlling light in WDM systems is the optical filter. There are mainly two classes of optical filters.

1) Finite impulse response (FIR) / moving average (MA) filters: filters that do not rely on any feedback mechanism, i.e., do not rely on optical reflections. These filters are sometimes called feed–forward and examples are Mach-Zehnder based filters and waveguide grating routers (WGRs).

2) Infinite impulse response (IIR) / autoregressive (AR) filters: filters inherently based on multiple reflections. Examples of these include fiber bragg gratings (FBGs), thin film filter (TFFs), nad optical all-pass filters (APFs).

The description of some of the most common optical filters [2] is given by : plane grating A typical reflective grating consists of a mirrored surface with tiny periodically located grooves. When illuminated, the light reflected from one groove interferes with the light reflected from other grooves, resulting in constructive and destructive interference. The wavelength dependence of the interference patterns are exploited to separate the different wavelengths which are detected for example by using a photodiode.

Figure 2.6: Plane grating.

Fabry-Perot interferometer

This principle of this filter was invented in 1898 by the French physicists Charles Fabry and Alfred Perot. The principle is still the same; two highly reflective parallel mirrors are separated by a small distance. Most of the light which encounters the first mirror is reflected, but some of it transmits, travel through the cavity [the space between the mirrors, often filled with some kind of dielectric e.g. liquid crystals (LCs)], and strikes the second mirror. At the second mirror most of the light is reflected, while some transmits.

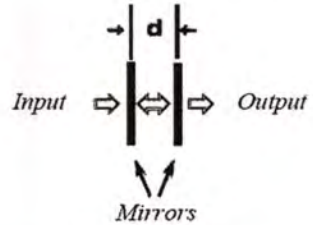

Figure 2.7: Fabry-Perot interferometer.

The reflected light travels backwards, hitting the first mirror, where some of it again reflects and some transmits. The result is that depending on the spacing and index of refraction between the mirrors, at some wavelengths the multiple reflections interfere constructively. At these wavelengths the cavity "resonates", so that the light passes through. For other wavelengths the transmitted waves add out of phase and the reflected waves add in phase. At these wavelengths the interferometer's overall transmission is low, and the overall reflectivity is high.

Fiber Bragg grating [3]

These types of filters consist of a region in which the index of the fiber varies periodically between high and low, and they are formed in optical fibers by exposing the fiber to interferometric patterns from an ultraviolet (UV) laser. As in the Fabry-Perot interferometer, multiple reflected and transmitted waves result. For a specific wavelength the reflected waves all add in phase, and at this wavelength the grating appears to be highly reflective, while transmitting all the others.

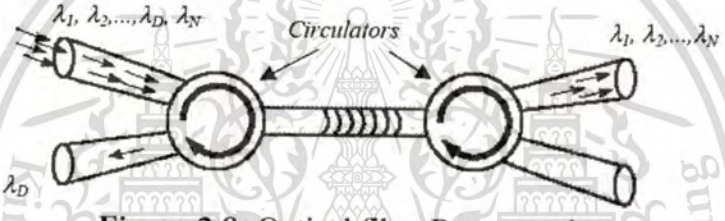

Figure 2.8: Optical fiber Bragg grating.

Arrayed waveguide grating (AWG) [4]

The most common filter in optical telecommunications is this type of filter. The AWG uses an array of single mode waveguides in which the lengths of adjacent waveguides differ by a fixed amount. The input light from a single fiber illuminates all these waveguides. Because of the different lengths of the waveguides, the phase of the light (at the output end of the array of waveguides) varies by a fixed amount, from one waveguide to the next. This variation results in a wavelength dependent phase front that is similar to the one from a plane grating. This pattern is then arranged so that different wavelengths illuminate different output fibers. The AWG can serve as a wavelength multiplexer as well as a demultiplexer.

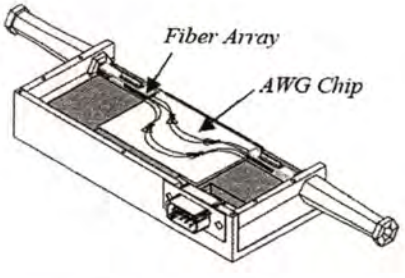

Figure 2.9: Packaged arrayed waveguide grating.

Mach-Zehnder interferometer (MZI)

This filter consists of a pair of couplers connected by two paths of unequal length. Group velocity dispersion in the optical paths of different lengths results in some wavelengths being output to the top port, and other wavelengths being output to the bottom port.

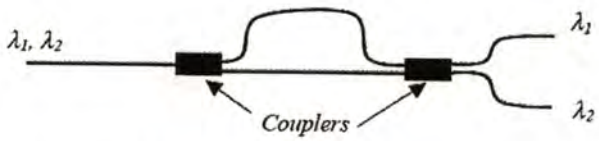

Figure 2.10: Mach-Zehnder interferometer.

Thin film dielectric interference filter

This filter requires the deposition of many layers of coating to create narrow-band filters. A typical filter with a 3 dB bandwidth OF 100 GHz requires more than a hundred layers of coating. With so many layers being deposited, errors caused by local film thickness variation and alternation in density increase, reducing the yield of useful filters. A transmitted beam that goes through a filter is composed of multiple sub-beams, each having a slightly different travel time, which adds dispersion to the data signal.

2.3 Optical Add/Drop Filter

Unlike Fabry-Perot cavities, Bragg gratings, and distributed feedback waveguide devices, the ring geometry permits more than one waveguide to be coupled to the ring resonator. This in return allows multiple input/output accessibility and no need for external circulators to manipulate the input, reflected and throughput data streams. For instance, if one more waveguide is coupled to the filter described earlier, an optical add/drop filter is obtained, as shown in Figure. 3.10.

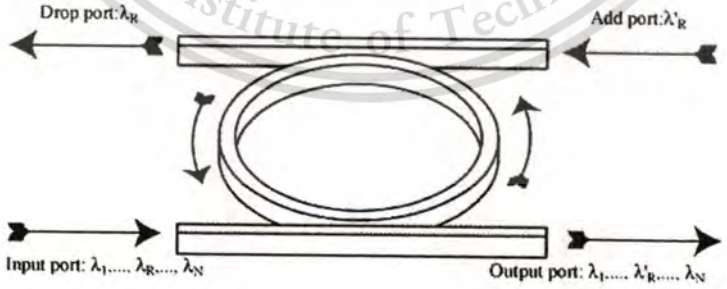

Figure 2.11: Schematic diagram for a ring resonator coupled to two waveguides,in an add/drop filter configuration.

An incident optical signal composed of multiple wavelengths $(\lambda_1,\ldots,\lambda_R,\ldots,\lambda_N)$ at the input port coupled into the ring and for a resonant wavelength (λ_R), the energy builds up in the resonator despite the small coupling and eventually the signal is coupled into the drop port. Symmetrically, a new signal at resonant

wavelength (λ_R') at the add port couples to the output port through the ring. As a result, such a configuration constitutes a very compact add/drop filter where a channel can be dropped from the WDM spectrum and replaced by a new signal on the same channel. Note that waves with a wavelength away from resonance will not repeat themselves in the ring and the coupled field interferes destructively with the wave in the resonator leading to little energy in the resonator and little dropped power. Residual dropped power at non-resonant wavelengths is possible due to imperfections and can induce inter-band crosstalk that is detrimental to WDM applications. Moreover, if the input channel at λ_R is not completely extinguished, intra-band crosstalk will result. These issues will be studied and can be theoretically overcome by varying coupling parameters, inducing loss/gain in the ring and inserting additional rings between the two waveguides.

2.4 Microring Resonators

A ring resonator is simply a waveguide shaped into a ring structure as shown in Figure. 2.12. When an input electric field, E_i is coupled to the ring waveguide through an external bus waveguide, a positive feedback is induced and the field inside the ring resonator, E_{r2} starts to build up. Coupling between the straight and the ring waveguide is achieved through the evanescent wave. Therefore, the gap and coupling length between them determine how much power is coupled from the straight waveguide to the ring waveguide and vise versa. The feedback mechanism is simply induced by the ring waveguide and therefore there is no need for any Bragg gratings, mirrors, or distributed feedback waveguides which are more difficult to fabricate. In such configuration, only certain wavelengths will be allowed to resonate inside the ring waveguide, thus frequency selectivity is obtained.

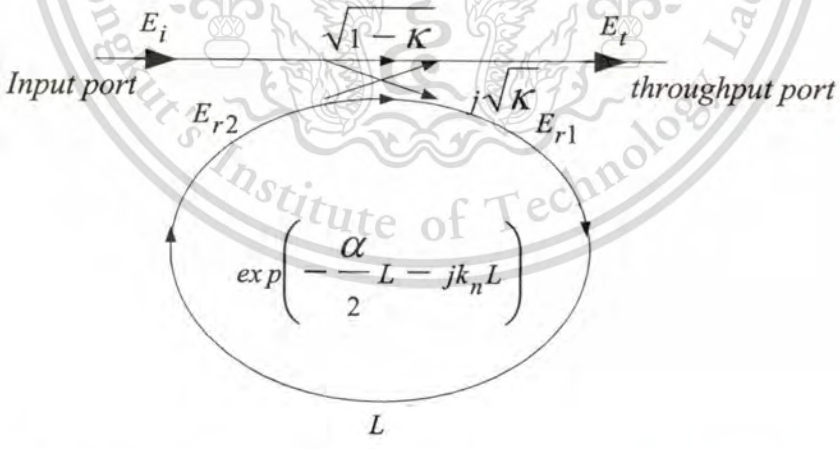

Figure 2.12: Schematic diagram for a ring resonator coupled to a single waveguide.

The transfer function of this configuration is derived using Z-transform analysis. The circumference of the ring is L ($L = 2\pi R$, the radius is R), the coupling coefficient of the coupler is κ. The Z-transform parameter is represented by $z^{-1} = \exp^{-jk_nL}$ where $k_n = \frac{2\pi}{\lambda} n_{eff}$ is the propagation constant and n_{eff} is the effective

index of the waveguide. The one round trip loss is $a = \exp^{-\alpha L/2}$, α is the intensity attenuation coefficient inside the waveguide [unit $length^{-1}$]. The transmitted or throughput field at the output of the straight waveguide, E_t and inserted electric field, E_i relations can be derived as followed:

$$E_t = (1-\gamma)^{1/2} \times \left[E_i \cdot \sqrt{1-\kappa} + j \cdot E_{r2}\sqrt{\kappa}\right]. \tag{2.19}$$

$$E_{r1} = (1-\gamma)^{1/2} \times \left[j \cdot E_i \cdot \sqrt{\kappa} + E_{r2} \cdot \sqrt{1-\kappa}\right]. \tag{2.20}$$

$$E_{r2} = E_{r1} \cdot a\, z^{-1}. \tag{2.21}$$

Using these equations, E_t / E_i can be calculated:

$$\frac{E_t}{E_i} = (1-\gamma)^{1/2} \times \left[\frac{\sqrt{1-\kappa} - (1-\gamma)^{1/2} \cdot a\, z^{-1}}{1-(1-\gamma)^{1/2} \cdot \sqrt{1-\kappa} \cdot a\, z^{-1}}\right]. \tag{2.22}$$

The transfer function in Eq. (2.22) indicates that a ring resonator is very similar to a Fabry-Perot cavity. In the particular case shown in Figure. 2.12, the corresponding Fabry-Perot cavity would have an input mirror with a field reflectivity and a fully reflecting output mirror. However, the field propagating inside the ring cavity is a traveling wave in contrast to the Fabry-Perot cavity which resonates a standing wave.

In the following, new parameter will be used for simplification:

$$\begin{aligned} D &= (1-\gamma)^{1/2} \\ x &= D \cdot \exp^{-\alpha L/2} \\ y &= \sqrt{1-\kappa} \\ \phi &= k_n \cdot L \end{aligned} \tag{2.23}$$

The intensity relation for the output port is given by:

$$T = \frac{I_t}{I_i}(\phi) = \left|\frac{E_t}{E_i}\right|^2 = D^2 \cdot \left[1 - \frac{(1-x^2)\cdot(1-y^2)}{(1-x\cdot y)^2 + 4\cdot x\cdot y\cdot sin^2\left(\frac{\phi}{2}\right)}\right]. \tag{2.24}$$

The transmission spectrum of a single ring resonator is shown in Figure. 2.12. The maximum and minimum transmission is calculated, using:

$$T_{\max} = D^2 \cdot \frac{(x+y)^2}{(1+x\cdot y)^2}. \tag{2.25}$$

$$T_{\min} = D^2 \cdot \frac{(x-y)^2}{(1-x\cdot y)^2}. \tag{2.26}$$

The minimum transmission $T_{\min}$, occurs at resonant point when the circumference of the ring L, is an integral number of guide wavelength which is defined by

$$\phi = k_n \cdot L = 2m\pi, \qquad m = integer$$

$$m \cdot \lambda_m = n \cdot L . \tag{2.27}$$

Here, m is the mode number, λ_m is the resonant mode wavelength.

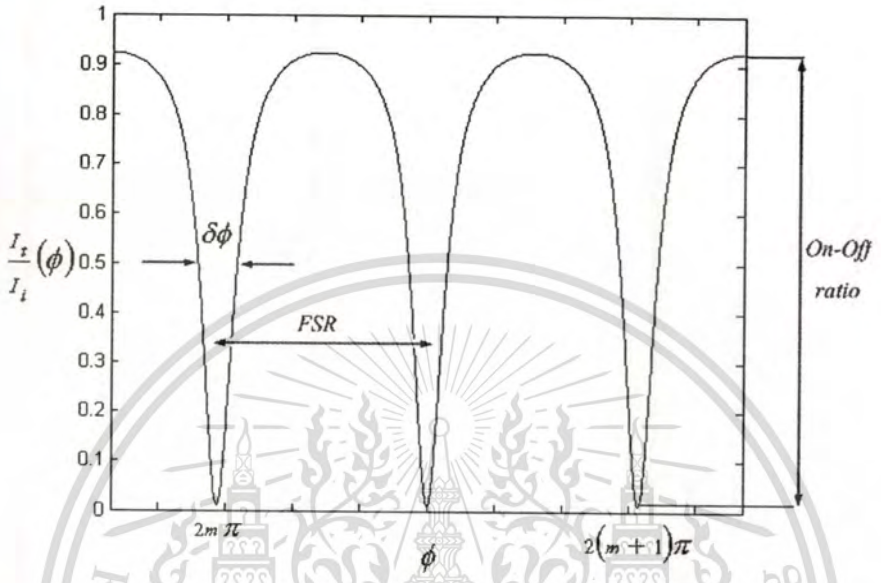

Figure 2.13: Transmission characteristic of a single ring resonator.

The on-off ratio for the throughput and drop port, which is the ratio of the on-resonance intensity to the off- resonance intensity which is given by:

$$ON - OFF\ ratio = \frac{T_{max(throughput\ port)}}{T_{min(drop\ port)}} . \tag{2.28}$$

The on-off ratio will become maximum if

$$T_{\min} = 0 \Rightarrow x = y \Rightarrow \alpha = -\frac{1}{L} \cdot \ln(\frac{1-\kappa}{D^2}) . \tag{2.29}$$

This relationship is also referred to as the critical coupling. The maximum on-off ratio [$\frac{I_t}{I_i}(2m\pi) = 0$, Figure. 2.13] can be achieved by varying the coupling factor κ or the intensity attenuation coefficient α (Eq. 2.29). The value of α can only be changed severely by the implementation of an SOA within the ring resonator or using an all-active ring resonator.

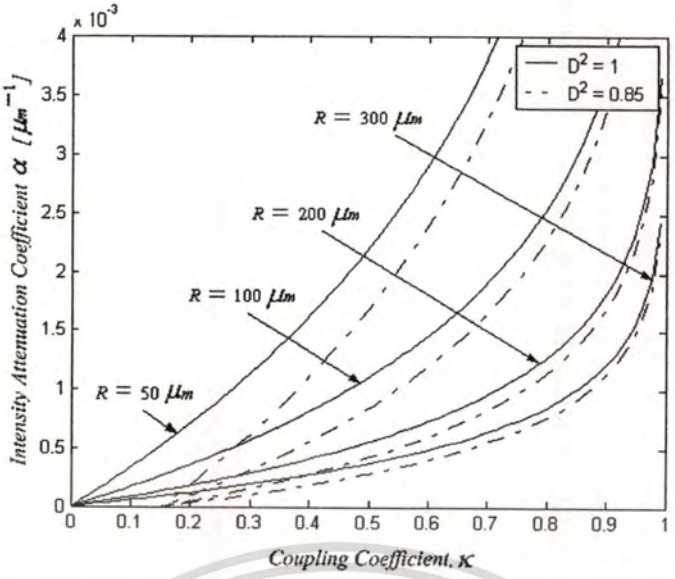

Figure 2.14: Evaluation of the ideal coupling coefficient κ for a given intensity attenuation coefficient α.

The ideal intensity attenuation coefficient α for single ring resonator to achieve a maximum on-off ratio $[\frac{I_t}{I_i}(2m\pi)=0]$, for example, with a radius of R=100 μm, a power coupling coefficient of $\kappa = 0.5$, an intensity insertion loss of the coupler of $D^2 = 85\%$ ($\gamma = 15\%$) is taken from the diagram (Figure. 2.13) to be $\alpha = 0.0008\,\mu m^{-1}$.

CHAPTER 3
OPTICAL SOLITON

The basic equation governing the propagation of pulses in optical fibers is known as the nonlinear Schrödinger equation, or NLS equation for short. It is of fundamental importance to almost everything we shall discuss in this book. In this chapter we shall derive that equation and examine some of its most immediate consequences. Before beginning a detailed study, however, it is useful to have a first look at this innocent-looking equation and its most significant properties. The NLS equation is

$$-i\frac{\partial u}{\partial z}=\frac{1}{2}\frac{\partial^2 u}{\partial t^2}+|u|^2 u \tag{3.1}$$

As its name suggests, Eq. (3.1) is similar to the well-known Schrödinger equation of quantum mechanics. Here, of course, it has nothing to do with quantum mechanics. Rather, it is just Maxwell's equations, adapted to field propagation in single-mode optical fiber. However, the analogy to quantum mechanics may be instructive to some, as the nonlinear term (the second on the right) is analogous to a negative potential energy, which allows the possibility of self-trapped pulse solutions. These are the solitons, which are the central concern of this book.

In a single-mode fiber, there is only one possible spatial behavior in the transverse dimensions x and y, so that we need to deal only with appropriate averages of the field quantities over those dimensions. Thus, the NLS equation involves only distance along the propagation direction, z, and time, t. The complex quantity u(z, t) is proportional to the light field, with the "central optical frequency" (a frequency arbitrarily chosen somewhere near the mean frequency of the pulse) and the mean time of flight to location z removed; the latter is done so that the pulse always remains in view. The absolute magnitude of u represents the amplitude envelope of the pulse. The phase of u, both in its average change with z and in its variation across the pulse, is equally important in determining the way a pulse propagates.

When polarization is an issue, two functions u(z, t) are required, one for each of the two possible (orthogonal) polarization states. Mild birefringence of the (nominally cylindrical) fibers tends to make the path-average behavior of these two functions nearly identical, however, so usually just one u can be taken as representative, to tell us all we really want to know.

The solutions u(z, t) of Eq. (3.1) directly yield the temporal form of the pulse as seen by an observer at the location z; thus, in the context of telecommunications, time and distance are typically on the scales of picoseconds and kilometers, respectively. Of course, u can be easily transformed to yield the complementary picture where the observer takes a snapshot of the pulse (i.e., observes it as a function of z) at various different times. In the latter picture, one has such familiar terms as group velocity and group velocity dispersion. In the former picture, one has (transit) time delay and time delay dispersion. In this book, as in almost all work on pulse propagation in fibers, we shall adhere to this former view.

It should be emphasized that t in Eq. (3.1) represents retarded time, i.e., ordinary time, but with the transit time delay of a pulse at the central frequency subtracted off. Also, in the frequency spectrum of a pulse satisfying Eq. (3.1),

the frequency is the actual frequency minus the central frequency. This makes it much easier to see changes in the pulse shape and spectrum, and deviations from the expected arrival time of a pulse, especially after it has traveled a great distance down the fiber.

The first term on the right of Eq. (3.1), the one involving the second derivative with respect to time, describes the effects of chromatic dispersion. (This is more evident in the Fourier transform of the equation, where the second derivative with respect to time becomes more simply minus the square of the frequency.) It is important to note that this linear term, when acting by itself, does nothing to change the frequency spectrum of the pulse. It serves only to broaden (or narrow) the pulse in time.

The second term on the right of Eq. (3.1) is the nonlinear term. Note that it is just the pulse's intensity envelope times u itself. It is based on the fact that the index of refraction, as will be detailed shortly, is dependent on the light intensity. It is important to note that this term, when acting by itself, does nothing to change the pulse shape in time. It serves only to broaden (or narrow) the pulse in the frequency domain.

We will study many modifications of the NLS equation pertinent to light field propagation in glass fibers. The foremost is the power loss (or gain) in the fiber. Loss is primarily due to absorption and scattering. Gain can be incorporated in the fiber, as we shall detail later. When loss or gain is taken into account, Eq. (3.1) becomes

$$-i\frac{\partial u}{\partial z}=\frac{1}{2}\frac{\partial^2 u}{\partial t^2}+|u|^2 u-i\frac{1}{2}\alpha u \tag{3.1a}$$

where a positive or negative value of α implies, respectively, gain or loss. The factor of one-half in the α term causes α itself to represent power (or energy) loss or gain per unit length.

Equation (3.1) is applicable when the loss/gain term can be neglected (as can happen, even in very long fibers, through the application of loss-canceling optical gain). It is a much studied equation, as it is one of the few that support solitons. Solitons are a class of solitary wave pulses that can pass through one another with no scattering. Zakarov and Shabat [5,6] most elegantly showed that the general solution of Eq. (3.1) consists of solitons accompanied by smaller dispersive fields called "radiation." They used a method called the "inverse scattering transform," which is a kind of nonlinear Fourier transform.

$$u(z,t)=\sec h(t)\exp\left(\frac{iz}{2}\right) \tag{3.2}$$

known as the fundamental soliton. It is a particular pulse of unit amplitude whose mean frequency is the central frequency. [For the benefit of those unfamiliar with it, the hyperbolic secant (sech) function, defined as sech(t) = 2/[exp(t)+exp(−t)], has a shape similar to the more familiar Gaussian function, but it has a narrower peak and broader wings.] Note that since the phase term in Eq. (3.2) has no dependence on t, the soliton is completely nondispersive. That is, its shape does not change with z either in the temporal domain, as shown explicitly here, or in the frequency domain. It happens that the Fourier transform of a sech function is also a sech function. In particular, the Fourier transform of Eq. (3.2) is proportional to sech(πω/2). This invariance with propagation occurs, for the soliton, since the dispersive and nonlinear terms of the NLS equation cancel each other's effects, leaving only a phase shift of the whole pulse. It may at first seem somewhat mysterious that the dispersive term, which affects the pulse only in the time domain, can cancel the nonlinear term, which affects the pulse only in the frequency domain. As we shall soon see, however, the explanation of this seeming

paradox is quite straightforward, since over very short distances both terms modify only the phase of the pulse.

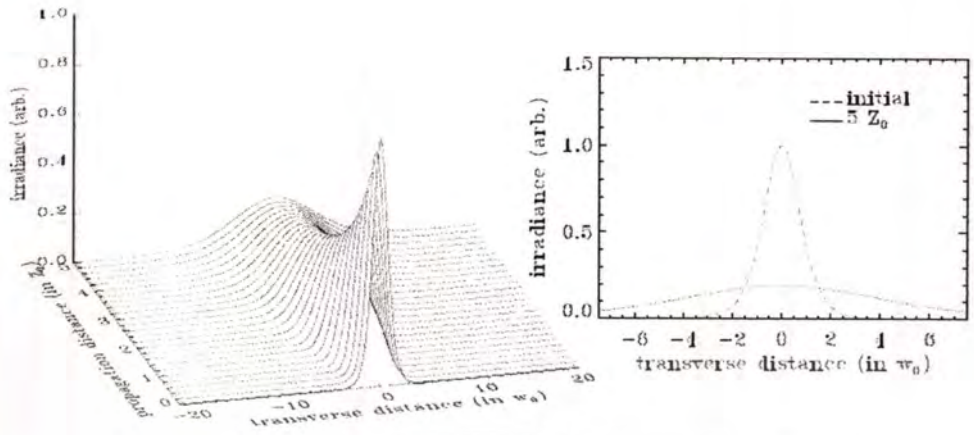

Figure 3.1: Diffraction of a beam of initial sech(x/ω_0).[7]

Figure 3.2: Spatial soliton beam of initial sech(x/ω_0) amplitude profile.[7]

At this point the reader may well ask, "Where are the fundamental physical constants, such as the speed of light or the nonlinear index coefficient, and where are the parameters particular to the problem, such as the pulse width and power, and the fiber's dispersion parameter and core area." The answer is that they have been incorporated into definitions of special "soliton units" used to measure distance, time, and power, in such a way that the NLS equation has the simple appearance of Eq. (3.3). This scheme of special units provides yet another simplification, this time to facilitate solution through numerical simulation, and by often enabling interpretation of the results in terms of a range of pulse parameters, instead of for just one particular set. The scaling of the soliton units with pulse and fiber parameters is of fundamental importance, both for understanding and for their engineering consequences. Thus we shall examine that behavior thoroughly in the following sections.

The theme of this book is the study of solitons in communications systems. Thus the pulses we are concerned with are always "narrow band" in the sense that their spectral width is much less than their mean frequency. As such, we note that the NLS equation, either as displayed in Eq. (1.1), or with minor modification, tends to embrace all dispersive and nonlinear phenomena that may be of interest here. For example, the basic NLS equation supposes that a quadratic function adequately describes the dispersion relation k(ω) over the bandwidth of concern. For shorter pulses, this may not be a completely adequate description. Usually, however, departures from quadratic dispersion are small and can be treated as perturbations of the basic equation. Another example is the Raman effect, which can transfer energy from higher frequencies to lower frequencies within a pulse or between pulses of different frequencies. The NLS equation supposes that the nonlinearity of the refractive index is instantaneous. The Raman effect can be heuristically regarded as resulting from a small delay in the establishment of the nonlinear index. For pulses longer than a few picoseconds in typical glass fibers, these effects are small and can often be accounted for in simple ways, but they cannot be neglected. Other yet smaller effects are present, but can usually be ignored for our purposes.

3.1 Self-Phase Modulation (SPM)

The need of communication is an all time need of human beings. For communication some channel is needed. Fiber is one channel among many other channels for communication. The dispersion phenomenon is a problem for high bit rate and long haul optical communication systems. An easy solution of this problem is optical solitons–pulses that preserve their shape over long distances. Soliton based optical communication systems can be used over distances of several thousands of kilometers with huge information carrying capacity by using optical amplifiers.

Self-phase modulation (SPM) is the frequency change caused by a phase shift induced by the pulse itself. SPM arises because the refractive index of the fiber has an intensity dependent component. When an optical pulse travels through the fiber, the higher intensity portions of an optical pulse encounter a higher refractive index of the fiber compared with the lower intensity portions. The leading edge will experience a positive refractive index gradient (*dn/dt*) and trailing edge a negative refractive index gradient (*-dn/dt*). This temporally varying index change results in a temporally varying phase change. The optical phase changes with time in exactly the same way as the optical signal [8, 9]. Different parts of the pulse undergo different phase shift because of intensity dependence of phase fluctuations. This results in frequency chirping. The rising edge of the pulse finds frequency shift in upper side whereas the trailing edge experiences shift in lower side as shown in Figure 3.1. Hence primary effect of SPM is to broaden the spectrum of the pulse, keeping the temporal shape unaltered.

For a fiber containing high-transmitted power, the phase (φ) introduced by a field $E = E_0 \cos(\omega t - kz)$ over a fiber length L is given by [10, 11],

$$\phi = \frac{2\pi}{\lambda}(n_l + n_{nl} I) L_{ef} f \tag{3.3}$$

where effective length $L_{eff} = \frac{(1-\exp(-\alpha L))}{\alpha}$. Linear and nonlinear refractive indices are n_l and n_{nl} respectively and α is attenuation coefficient. The first term on right hand side refers to linear portion of phase constant (φ_l) and second term provides

nonlinear phase constant (φ_{nl}). This variation in phase with time is responsible for change in frequency spectrum.

For a Gaussian pulse, the optical carrier frequency ω (say) is modulated and the new instantaneous frequency becomes,

$$\omega' = \omega_0 + \frac{d\phi}{dt} \tag{3.4}$$

The sign of the phase shift due to SPM is negative because of the minus sign in the expression for phase i.e., $(\omega t - kz)$. Using equations (3.3) and (3.4) ω' can be written as,

$$\omega' = \omega_0 - \frac{2\pi}{\lambda} L_{eff} n_{nl} \frac{dI}{dt} \tag{3.5}$$

At leading edge of the pulse $\frac{dI}{dt} > 0$;

$$\omega' = \omega_0 - \omega(t) \tag{3.6}$$

And at trailing edge $\frac{dI}{dt} < 0$;

$$\omega' = \omega_0 + \omega(t) \tag{3.7}$$

where,

$$\omega(t) = \frac{2\pi}{\lambda} L_{eff} n_{nl} \frac{dI}{dt} \tag{3.8}$$

Thus chirping phenomenon (frequency variation) is generated due to SPM, which leads to the spectral broadening of the pulse without any change in temporal distribution. The SPM induced chirp can be used to modify the pulse broadening effects of dispersion. SPM phenomenon also can be used in pulse compression. In the wavelength region where chromatic dispersion is positive, the red-shifted leading edge of the pulse travels slower and moves toward the center of pulse. Similarly, the blue shifted trailing edge travels faster, and also moves toward the center of the pulse. In this situation SPM causes the pulses to narrow. Another simple pulse compression scheme is based on filtering self-phase modulation-broadened spectrum [12, 13].

The performance of self-phase modulation-impaired system can be improved significantly by adjusting the net residual (NRD) of the system. For SPM-impaired system the optimal NRD can be obtained by minimizing the output distortion of signal pulse. The NRD of SPM-impaired dispersion-managed systems can be optimized by a semi analytical expression obtained with help of perturbation theory. This method is verified by numerical simulations for many SPM-impaired systems [14, 15].

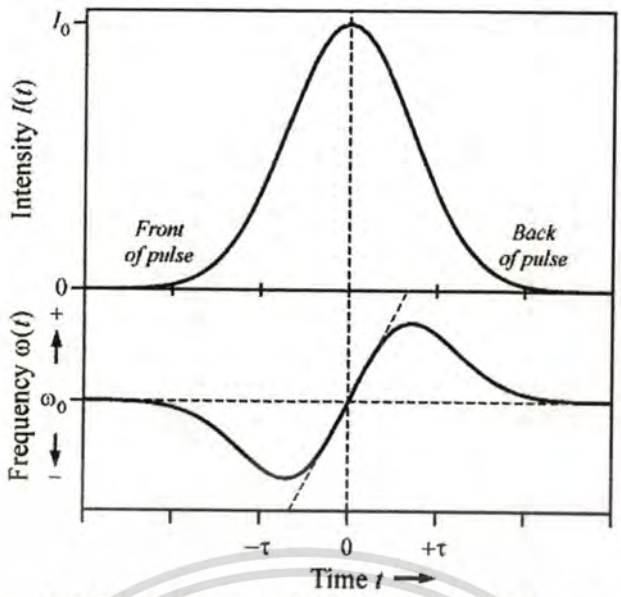

Figure 3.3: Spectral broadening of a pulse due to SPM.

3.2 Cross-Phase Modulation (XPM)

When two or more optical fields having different wavelengths propagate simultaneously inside a fiber, they interact with each other through the fiber nonlinearity. In general, such an interaction can generate new waves under appropriate conditions through a variety of nonlinear phenomena such as stimulated Raman or Brillouin scattering, harmonic generation, and four-wave mixing; these topics are covered in Stimulated Raman Scattering , Stimulated Brillouin Scattering and Parametric Processes. The fiber nonlinearity can also couple two fields through cross-phase modulation (XPM) without inducing any energy transfer between them. Cross-phase modulation is always accompanied by self-phase modulation (SPM) and occurs because the effective refractive index seen by an optical beam in a nonlinear medium depends not only on the intensity of that beam but also on the intensity of other copropagating beams [16].

The XPM-induced coupling among optical fields gives rise to a number of interesting nonlinear effects in optical fibers. This coupling between two fields of different wavelengths is considered in XPM-Induced Nonlinear Coupling where a set of two coupled nonlinear Schrödinger (NLS) equations is obtained.These equations are used in Coupled NLS Equations to discuss how the XPM affects the phenomenon of modulation instability. Similar to the analysis in Vector Modulation Instability, this instability can occur even in the normal-dispersion regime of an optical fiber. XPM-Paired Solitons focuses on soliton pairs whose members support each other through XPM. The effects of XPM on the shape and the spectrum of copropagating ultrashort pulses are described in Spectral and Temporal Effects. Several applications of XPM-induced coupling in optical fibers are discussed Applications of XPM.

This section extends the theory of pulse-propagation to the case of two optical pulses at different wavelengths copropagating inside a single-mode fiber. In general, the two optical fields can differ not only in their wavelengths but also in their states of polarization. To simplify the presentation, we first focus on the case in which the two optical fields at different wavelengths are linearly polarized along one of the principal

axes of a birefringent fiber. The case of arbitrarily polarized beams is discussed later in this section.

In the quasi-monochromatic approximation, it is useful to separate the rapidly varying part of the electric field by writing it in the form

$$E(r,t)=\tfrac{1}{2}\hat{x}\left[E_1\exp(-i\omega_1 t)+E_2\exp(-i\omega_2 t)\right]+c.c. \tag{3.9}$$

where $\hat{x}$ is the polarization unit vector, ω_1 and ω_2 are the carrier frequencies of the two pulses, and the corresponding amplitudes E_1 and E_2 are assumed to be slowly varying functions of time compared with an optical period. This assumption is equivalent to assuming that the spectral width of each pulse satisfies the condition $\Delta\omega j \ll \omega j$ (j = 1; 2), and holds quite well for pulse widths > 0.1 ps. Evolution of the slowly varying amplitudes E_1 and E_2.

To see the origin of XPM, we substitute Eq. (3.9) and find that the nonlinear polarization can be written as

$$P_{NL}(r,t)=\tfrac{1}{2}\hat{x}\begin{bmatrix}P_{NL}(\omega_1)\exp(-i\omega_1 t)+P_{NL}(\omega_2)\exp(-i\omega_2 t)\\ +P_{NL}(2\omega_1-\omega_2)\exp[-i(2\omega_1-\omega_2)t]\\ +P_{NL}(2\omega_2-\omega_1)\exp[-i(2\omega_2-\omega_1)t]\end{bmatrix}+c.c. \tag{3.10}$$

where the four terms depend on E_1 and E_2 as

$$P_{NL}(\omega_1)=\chi_{eff}\left(|E_1|^2+2|E_2|^2\right)E_1 \tag{3.11a}$$

$$P_{NL}(\omega_2)=\chi_{eff}\left(|E_2|^2+2|E_1|^2\right)E_2 \tag{3.11b}$$

$$P_{NL}(2\omega_1-\omega_2)=\chi_{eff}E_1^2E_2^* \tag{3.11c}$$

$$P_{NL}(2\omega_2-\omega_1)=\chi_{eff}E_2^2E_1^* \tag{3.11d}$$

with $\chi_{eff}=(3\varepsilon_0/4)\chi^{(3)}_{xxxx}$ acting as an effective nonlinear parameter.

The induced nonlinear polarization in Eq. (3.10) has terms oscillating at the new frequencies $2\omega_1-\omega_2$ and $2\omega_2-\omega_1$ These terms result from the phenomenon of four-wave mixing discussed in parametric processes. It is necessary to satisfy the phase-matching condition if the new frequency components are to build up significantly, a condition not generally satisfied in practice unless special precautions are taken. The four-wave-mixing terms are neglected in this chapter after assuming that phase matching does not occur. The remaining two terms provide a nonlinear contribution to the refractive index. This can be seen writing PNL(ω_j) in the form (j = 1;2)

$$P_{NL}(\omega_j)=\varepsilon_0\varepsilon_j^{NL}E_j \tag{3.12}$$

and combining it with the linear part so that the total induced polarization is given by

$$P(\omega_j) = \varepsilon_0 \varepsilon_j^{NL} E_j \tag{3.13}$$

Where

$$\varepsilon_j = \varepsilon_j^L + \varepsilon_j^{NL} = \left(n_j^L + \Delta n_j\right)^2 \tag{3.14}$$

n_j^L is the linear part of the refractive index and Δn_j is the change induced by the third-order nonlinear effects. Using the approximation $\Delta n_j \ll n_j^L$, the nonlinear part of the refractive index is given by (j = 1;2)

$$\Delta n_j \approx \varepsilon_j^{NL} \Big/ 2n_j \approx n_2 \left(\left|E_j\right|^2 + 2\left|E_{3-j}\right|^2\right) \tag{3.15}$$

where $n_1^L \approx n_2^L = n$ has been assumed. The nonlinear parameter n_2 is defined as in

$$n_2 = \frac{3}{8n}\mathrm{Re}\left(\chi_{xxxx}^{(3)}\right) \text{ and } \alpha_2 = \frac{3\omega_0}{4nc}\mathrm{Im}\left(\chi_{xxxx}^{(3)}\right)$$

Equation (3.9) shows that the refractive index seen by an optical field inside an optical fiber depends not only on the intensity of that field but also on the intensity of other copropagating fields [17]–[19]. As the optical field propagates inside the fiber, it acquires an intensity-dependent nonlinear phase shift

$$\phi_j^{NL}(z) = \left(\omega_j / c\right)\Delta n_j z = n_2\left(\omega_j / c\right)\left(\left|E_j\right|^2 + 2\left|E_{3-j}\right|^2\right)z \tag{3.16}$$

where j = 1 or 2. The first term is responsible for SPM. The second term results from phase modulation of one wave by the co propagating wave and is responsible for XPM. The factor of 2 on the right-hand side of Eq. (3.16) shows that XPM is twice as effective as SPM for the same intensity [6]. Its origin can be traced back to the number of terms that contribute to the triple sum implied in $P_{NL}(r,t) = \varepsilon_0 \chi^{(3)} \vdots E(r,t)E(r,t)E(r,t)$. Qualitatively speaking, the number of terms doubles when the two optical frequencies are distinct compared with that when the frequencies are degenerate. The XPM-induced phase shift in optical fibers was measured as early as 1984 by injecting two continuous-wave (CW) beams into a 15-km-long fiber [19]. Soon after, picosecond pulses were used to observe the XPM-induced spectral Optical Solitons , Polarization Effects and Cross-Phase Modulation.

3.3 Dark and Brigh Soliton

Dark solitons correspond to the solutions of Schrödinger with sgn (β_2) = 1 and occur in the normal-GVD region of fibers. They were discovered in 1973 and have attracted considerable attention since then . The intensity profile associated with such solitons exhibits a dip in a uniform background, hence the name dark soliton. Pulse-like solitons discussed are called bright to make the distinction clear. The NLS equation describing dark solitons is obtained from Schrödinger by changing the sign of the time-derivative term and is given by

$$i\frac{\partial u}{\partial \xi}-\frac{1}{2}\frac{\partial^2 u}{\partial \tau^2}+|u|^2 u=0 \tag{3.17}$$

Similar to the case of bright solitons, the inverse scattering method has been used [20] to find dark-soliton solutions of Schrödinger by imposing the boundary condition that $|u(\xi,\tau)|$ tends toward a constant nonzero value for large values of $|\tau|$. Dark solitons can also be obtained by assuming a solution of the form $u(\xi,\tau)=V(\tau)\exp[i\phi(\xi,\tau)]$, and then solving the ordinary differential equations satisfied by V and φ . The main difference compared with the case of bright solitons is that $V(\tau)$ becomes a constant (rather than being zero)

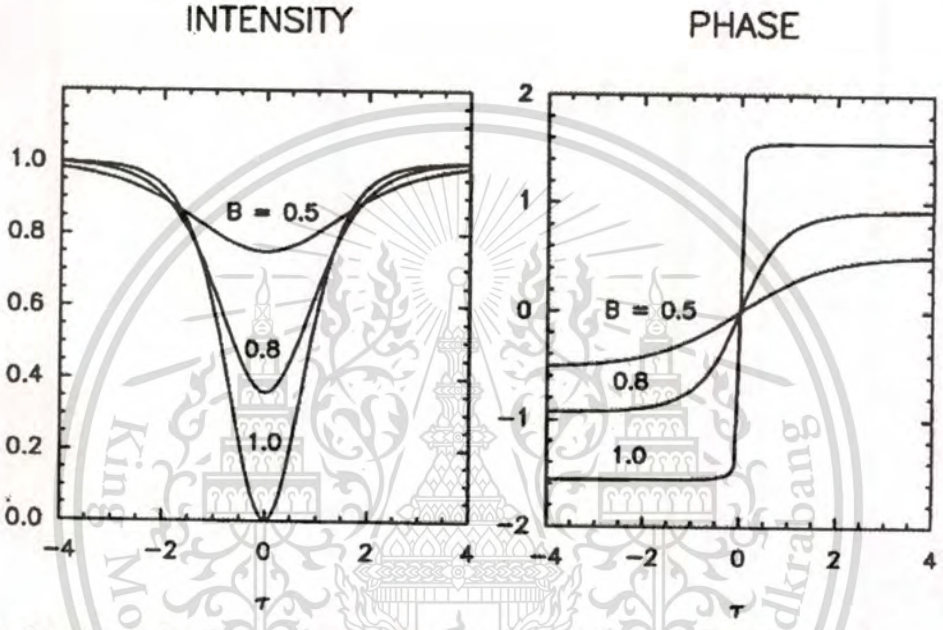

Figure 3.4: Intensity and phase profiles of dark solitons for several values of the blackness parameter B.

as $|\tau|\to\infty$. The general solution can be written as [21]

$$|u(\xi,\tau)|\equiv V(\tau)=\eta\left\{1-B^2\sec h^2\left[\eta B(\tau-\tau_s)\right]\right\}1/2 \tag{3.18}$$

with the phase given by

$$\phi(\xi,\tau)=\tfrac{1}{2}\eta^2\left(3-B^2\right)\xi+\eta\sqrt{1-B^2}\,\tau+\tan^{-1}\left(\frac{B\tanh(\eta B\tau)}{\sqrt{1-B^2}}\right) \tag{3.19}$$

The parameters η and τ_s represent the soliton amplitude and the dip location, respectively. Similar to the bright-soliton case, τ_s can be chosen to be zero without loss of generality. In contrast with the bright-soliton case, the dark soliton has a new parameter B. Physically, B governs the depth of the dip $(|B|\le 1)$. For $|B|$ = 1, the intensity at the dip center falls to zero. For other values of B, the dip does not go to zero. Dark solitons for which $|B|$ < 1 are called gray solitons to emphasize this feature; the parameter B

governs the blackness of such gray solitons. The $|B| = 1$ case corresponds to a black soliton.

For a given value of η, Eq. (2.19) describes a family of dark solitons whose width increases inversely with B. Figure 3.2 shows the intensity and phase profiles of such dark solitons for several values of B. Whereas the phase of bright solitons remains constant across the entire pulse, the phase of dark soliton changes with a total phase shift of $2\sin^{-1}B$, i.e., dark solitons are chirped. For the black soliton ($|B| = 1$), the chirp is such that the phase changes abruptly by π in the center. The phase change becomes more gradual and smaller for smaller values of $|B|$. The time-dependent phase or frequency chirp of dark solitons represents a major difference between bright and dark solitons. One consequence of this difference is that higher-order dark solitons neither form a bound state nor follow a periodic evolution pattern discussed in Higher-Order Solitons in the case of bright solitons.

Dark solitons exhibit several interesting features [21]. Consider a black soliton whose canonical form is obtained from Eq. (5.3.2), choosing $\eta = 1$ and B = 1, and given by

$$u(\xi,\tau) = \tanh(\tau)\exp(i\xi) \tag{3.20}$$

where the phase jump of π at $\tau = 0$ is included in the amplitude part. Thus, an input pulse with "tanh" amplitude, exhibiting an intensity "hole" at the center, would propagate unchanged in the normal-dispersion region of optical fibers. One may ask, in analogy with the case of bright solitons, what happens when the input power exceeds the N = 1 limit. This question can be answered by solving Eq. (3.17) numerically with an input of the form $u(0,\tau) = N\tanh(\tau)$. Figure 3.3 shows the evolution pattern for N = 3; it should be compared with Fig. 3.2 where the evolution of a third-order bright soliton is shown. Two pairs of gray solitons appear and move away from the central black soliton as the propagation distance increases. At the same time, the width of the black soliton decreases [22]. This behavior can be understood by noting that an input pulse of the form $N\tanh(\tau)$ can form a fundamental black soliton of amplitude $N\tanh(N\tau)$ provided its width decreases by a factor of N. It sheds part of its energy in the process that appears in the form of gray solitons. These gray solitons move away from the central black soliton because of their different group velocities. The number of pairs of gray solitons is $N'-1$, where $N' = N$ for integer values of N or the next integer close to it when N is not an integer. The important feature is that a fundamental dark soliton is always formed for N > 1.

Experimental realization of dark solitons is possible only with a finite background instead of the infinite background associated with ideal dark solitons. In practice, a pulse with a narrow dip at its center is used to excite a dark soliton. Numerical calculations show that dark solitons with a finite background pulse exhibit propagation properties nearly identical to those with infinite background if the background pulse is wider by a factor of 10 or more compared with the soliton width [23]. Several techniques have been used to generate optical pulses with a narrow dip in the center [24]-[26]. Such pulses have been used for observing dark solitons in optical fibers. In one experiment , 26-ps input pulses (at 595 nm) with a 5-ps-wide central hole were launched along a 52-m fiber. In another experiment [25], the input to a 10-m fiber was a relatively wide 100-ps pulse (at 532 nm) with a 0.3-ps-wide hole that served as a dark pulse. However, as the phase was relatively constant over the hole width, such even-symmetry input pulses did

not have the chirp appropriate for a dark soliton. Nonetheless, output pulses exhibited features that were in agreement with the predictions of Eq. (3.17).

The odd-symmetry input pulses appropriate for launching a dark soliton were used in a 1988 experiment [26]. A spatial mask, in combination with a grating pair, was used to modify the pulse spectrum such that the input pulse had a phase profile appropriate for forming the dark soliton represented by Eq. (3.20). The input pulses obtained from a 620-nm dye laser were 2-ps wide with a 185-fs hole in their center. The central hole widened at low powers but narrowed down to its original width when the peak power was high enough to sustain a dark soliton of that width. The experimental results agreed with the theoretical predictions of Eq. (3.17) quite well. In this experiment, the optical fiber was only 1.2 m long. In a 1993 experiment [27], 5.3-ps dark solitons, formed on a 36-ps wide pulse obtained from a 850-nm Ti:sapphire laser, were propagated over 1 km of fiber. The same technique was later extended to transmit dark-soliton pulse trains at a repetition rate of up to 60 GHz over 2 km of fiber. These results show that dark solitons can be generated and maintained over considerable fiber lengths.

During the 1990s, several practical techniques were introduced for generating dark solitons. In one method, a Mach–Zehnder modulator, driven by nearly rectangular electrical pulses, modulates the CW output of a semiconductor laser [28]. In an extension of this method, electric modulation is performed in one of the two arms of a Mach–Zehnder interferometer. A simple all-optical technique consists of propagating two optical pulses, with a relative time delay between them, in the normal-GVD region of the fiber [29]. The two pulse broaden, become chirped, and acquire a nearly rectangular shape as they propagate inside the fiber. As these chirped pulses merge into each other, they interfere. The result at the fiber output is a train of isolated dark solitons. In another all-optical technique, nonlinear conversion of a beat signal in a dispersion-decreasing fiber is used to generate a train of dark solitons [30]. The technique is similar to that for generating a regular pulse train except that fiber GVD is chosen to be in the normal-dispersion regime everywhere along the fiber length. A 100-GHz train of 1.6-ps dark solitons was generated by using this technique and propagated over 2.2 km of (two soliton periods) of a dispersion-shifted fiber. Optical switching using a fiber-loop mirror, in which a phase modulator is placed asymmetrically, can also be used to generate dark solitons [31]. In another variation, a fiber with comblike dispersion profile was used to generate dark soliton pulses with a width of 3.8 ps at the 48-GHz repetition rate [32].

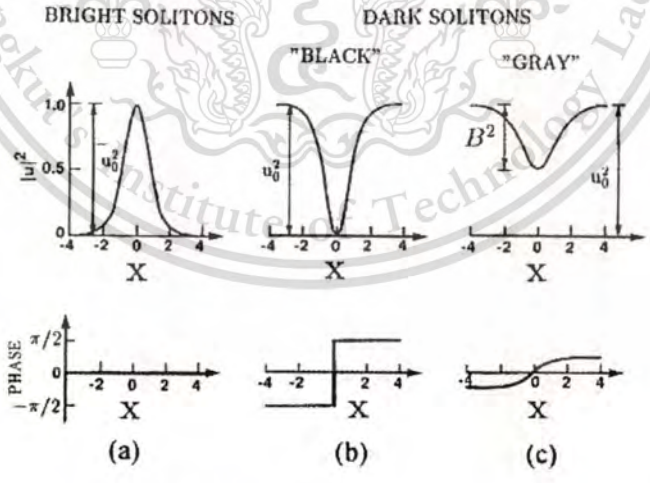

Figure 3.5: Intensity and phase as functions of normalized coordinate x for bright (a), black (b) and (c) gray solitons.

An interesting scheme uses electronic circuitry to generate a coded train ofdark solitons directly from the NRZ data in electric form [33]. First, the NRZ data and its clock at the bit rate are passed through an AND gate. The resulting signal is then sent to a flip-flop circuit in which all rising slopes flip the signal. The resulting electrical signal drives a Mach–Zehnder $LiNbO_3$ modulator and converts the CW output from a semiconductor laser into a coded train of dark solitons. This technique was used for data transmission, and a 10-Gb/s signal was transmitted over 1200 km by using dark solitons [34]. Another relatively simple method uses spectral filtering of a mode-locked pulse train by using a fiber grating [35]. This scheme has also been used to generate a 6.1-GHz train and propagate it over a 7-km-long fiber [36].

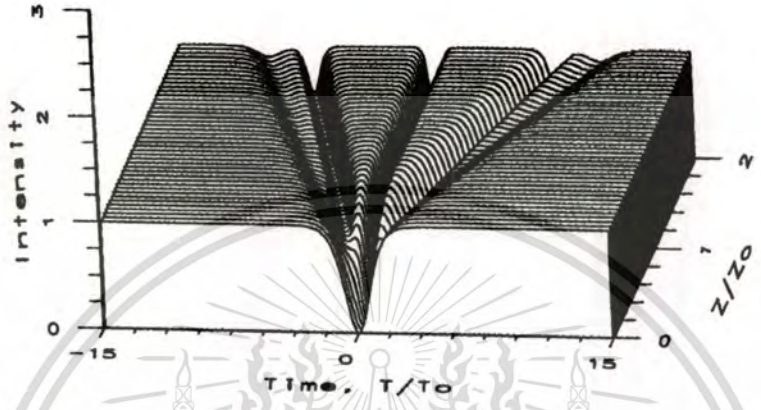

Figure 3.6: Evolution of a third-order dark soliton showing narrowing of the central dip and creation of two pairs of gray solitons.

Dark solitons remain a subject of continuing interest. Numerical simulations show that they are more stable in the presence of noise and spread more slowly in the presence of fiber loss compared with bright solitons. They are also relatively less affected by many other factors that have an impact on the use of bright solitons (amplifier-induced timing jitter, intrapulse Raman scattering, etc.). These properties point to potential application of dark solitons for optical communication systems. The reader is referred to Reference [37] for further details.

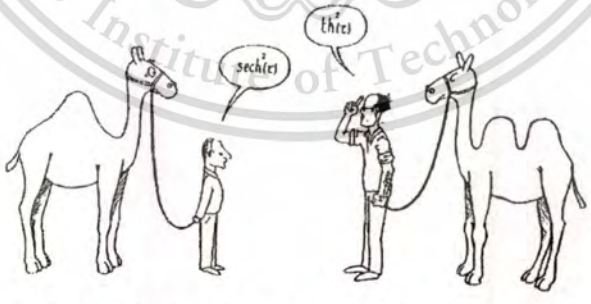

Figure 3.7: Do these 'animal' belong to the same soliton family.
(the drawing made by Marc Haelterman in 1989)

CHAPTER 4
OPTICAL SOLITONS IN NONLINEAR MICRORING RESONATORS

Optical ring resonators consist of a waveguide in a closed loop coupled to one or more input/output waveguides. When light of the appropriate wavelength is coupled to the loop by the input waveguide, it builds up in intensity over multiple round-trips due to constructive interference. It can then be picked up by a detector waveguide. Since only some wavelengths resonate in the loop, if function as a filter.

4.1 Optical Filters

Optical devices have been widely used in many applications, especially, in optical sensors and communications for two decades, where they have been involved in many areas of research. Up to date, the searching of new devices and technologies are still required. For instance, Yupapin and Suwancharoen have reported the use of chaotic signals generated by using a micro ring resonator for communication security [38],[39], where the transmission signals could be secured by using the analog or digital methods. The increasing in the channel capacity could be achieved by the technique called the chaotic encoding and packet switching [40], where the information could be secured with high capacity [41,42]. Chaiyasoonthorn et al [43] have reported the interesting results when the ultrafast pulse with pulse width of as could be easily generated by using a soliton pulse travelling in the nonlinear micro ring resonators. The interesting idea of such a scheme is that the system is very small which is capable to implement within a small instrument, whereas the required applications can be easily employed. Optical filter has also been the interesting devices that can be used to obtain the specific signals in terms of frequency, wavelength and time. In this work, we propose the interesting idea when the three forms of applications such as frequency filter, wavelength filter and fast light filter can be performed within a single system. Firstly, we present the application, when the technique of up-link and down-link can be integrated within a small device called the micro ring devices. However, there are several systems of optical wireless up-down-link converters reported [44,45], however, there is no such a system that can be performed the link within a single system. By using our system, the broad frequency bands can be generated and filtered within the single system. In application, the links can be performed by using the frequency bands generated by the technique called chaotic filtering, where the required frequency bands can be filtered and used. Results obtained have shown the good potential application for mobile telephone up-link and down-link device. Secondly, the broad wavelength generation can be generated within the micro ring device system, where the generation of a broad spectrum using the simple system is achieved. Furthermore, the generation of pulse width beyond pm using the proposed technique is also plausible. Finally, we propose the system of fast light generation, where fast light in the form of a soliton pulse can be performed, where the required signal can be obtained by using the chaotic filter behaviors. Results obtained have shown that the extremely fast switching within the attosecond (as) and beyond can be performed. However, the technique of fast light detection is not yet available. In practice, the technique known as slow light is recommended to perform the fast detection.

Optical soliton is recognized as a powerful laser pulse which can be used to generate the chaotic filter characteristics when propagates within the nonlinear micro ring resonators. When the soliton pulse is introduced into the multi-stage micro ring resonators as shown in Figure. 1, the input optical field (E_{in}) in the form of soliton pulse is expressed by an Eq. (4.1).

$$E_{in} = ASech\left[\frac{T}{T_0}\right]\exp\left[\left(\frac{z}{2L_D}\right)\right] \tag{4.1}$$

Where A and z are the optical field amplitude and propagation direction, respectively. $L_D = T_0^2/|\beta_2|i$ is the dispersion length of the soliton pulse. This solution describes a pulse that keeps its temporal width invariant as it propagates and thus is called a temporal soliton. T_o is known, once we can find the proper peak intensity $\left(|\beta_2/\gamma T_0^2|\right)$ that will make this pulse a soliton. For example, when the micro ring resonator at the 1550 nm wavelength, with a 12 W peak power, then $T_o = 50ns$ long, which is a pulse of about 2 mm length (in z). For the soliton pulse in the micro ring device, a balance should be achieved between the dispersion lengths $L_D = \frac{T_0^2}{|\beta_2|}$ and the nonlinear length $L_{NL} = \frac{1}{\gamma\psi_0}$, which are the length scales over which dispersive or nonlinear effects make the beam become wider or narrower. For a soliton pulse, there is balance between the two and hence $L_D = L_{NL}$.

$$n = n_0 + n_2 I = n_0 + (\frac{n_2}{A_{eff}})P, \tag{4.2}$$

where n_0 and n_2 are the linear and nonlinear refractive indexes, respectively. I and P are the optical intensity and optical field power, respectively. The effective mode core area of the device is A_{eff}. For the micro ring and nano ring resonators, the effective mode core areas range between 0.50 to 0.1 μm^2. Thus, the normalized output of the light field can be expressed as,

$$\left|\frac{E_{out}}{E_{in}}\right|^2 = (1-\gamma)^2\left[1 - \frac{\kappa\left[1-(1-\gamma)^2\tau^2\right]}{1+(1-\gamma)^2(1-\kappa)\tau - 2(1-\gamma)\sqrt{1-\kappa}\tau\cos\phi}\right]. \tag{4.3}$$

The close form of equation (4.3) indicates that a ring resonator in the particular case to very similar to a Fabry-Perot cavity, which has an input and output mirror with a field reflectivity, 1-κ, and a fully reflecting mirror. Where n_0 and n_2 are the linear and nonlinear refractive indices, the coupling coefficient is κ. Where $x = \exp^{-\frac{\alpha L}{2}}$ represents the one round-trip losses coefficient, $\phi_0 = kLn_0$ and $\phi_{NL} = kLn_2|E_1|^2$ ($E_1 = E_{in}$) are the linear and nonlinear phase shifts, $k = 2\pi/\lambda$ is the wave propagation number in a vacuum, respectively.

4.1.1 Frequency Filter

In this section, the key point is that the two different frequencies can be simultaneously filtered from the broad spectrum, where the up-down-link converters can be simultaneously operated within a single system. The proposed system of the simultaneous fast and slow light generation is as shown in Figure. 4.1 The single mode soliton pulse is become many modes (noisy signals) after circulating within the first micro ring device due to the nonlinear Kerr effects of light within the micro ring resonator. The chaotic filtering characteristics of the signals are formed by the other ring resonators within the system. However, in practice, the evidence of such a device in realistic application is required and found in reference [46]. By using the material parameters of *InGaAsP/InP*, the specified frequency bands can be obtained by using the appropriate ring parameters, finally, we end up with the following details. The soliton waveform with the center frequency at 2 GHz is input into the first micro ring resonator (R_1). The optical power is fixed to 550 mW, f_0 = 2 GHz, n_0 = 3.34, n_2 = 2.2 x 10^{-17} m^2W^{-1}, A_{eff} = 0.50 μm^2, α = 0.5 $dBmm^{-1}$, γ = 0.1, with 20,000 roundtrips. The chaotic signals are generated within the first ring (R_1), where the broad frequency band is obtained within the ring R_2. The clearer filtering signals are seen in ring R_3 and R_4.

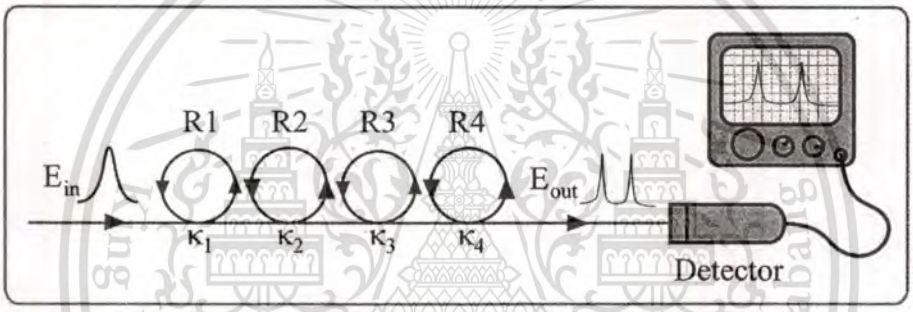

Figure 4.1: The schematic diagram of a simultaneous fast and slow light generation. Rs: ring radii, and κs : coupling coefficients.

4.1.2 Wavelength Filter

The remarkably simple system of the wavelength generation and filtering using a serial micro ring resonator is as shown in Figure 4.2. When a soliton pulse is input into the nonlinear Kerr effects medium (i.e. a nonlinear micro ring resonator), the nonlinear behavior known as chaos is introduced as shown in Figure 5.4 For instance, to make the system associate with the practical device [46], the selected parameters of the system are fixed to λ_0 = 1.55 μm, n_0 = 3.34 (InGaAsP/InP), A_{eff} = 0.50 μm^2, α = 0.02 $dBkm^{-1}$, γ = 0.1, and R_1 = 20 μm. The coupling coefficient of the micro ring resonator is fixed at κ = 0.5-0.9. The nonlinear refractive index is n_2 = 2.2 x 10^{-17} m^2/W. In this section, the system of the third harmonic generation consist the multi-stage micro ring resonators, where the ring radii are selected between 5 and 32 μm. The soliton pulse is coupled into the system with optical power of 1 W, coupling constants (kappa), κ = 0.5-0.9.The selected input pulse widths are 50 ns, 50 ps, 50 fs and 50 as, with the centre wavelength at 1550 nm. After the first micro ring resonator, the optical power is coupled into the second and third ring resonator, respectively. In this case, the wave guided loss used is 0.5 $dBmm^{-1}$. In Figure 4.1

when the input soliton with pulse width of 50 ns is input into the system, the chaotic behaviors are occurred within the micro ring resonators R_1 and R_2, when the ring radii are 20 and 5 μm, respectively.

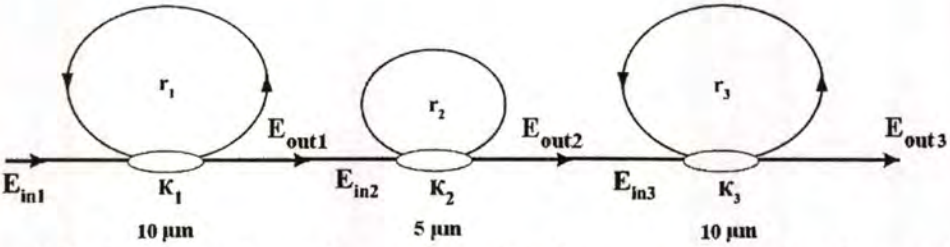

Figure 4.2: A schematic of the wavelength filter generation using the multi-stage micro ring resonators.

4.1.3 Ultra Fast Filter

The simple system of the fast light generation and filtering using a serial micro ring resonator is a similar system as shown in Figure 4.1: When a soliton pulse is input into the nonlinear Kerr effects medium, the nonlinear behavior of light traveling in a micro ring resonator is introduced. The parameters of the system are fixed to $\lambda_0 = 1.55$ μm, $n_0 = 3.34$ (InGaAsP/InP), $A_{eff} = 0.50$ μm2, $\alpha = 0.02$ dBkm^{-1}, $\gamma = 0.1$, and $R_1 = 10$ μm. The coupling coefficient of the micro ring resonator is fixed at $\kappa = 0.25$-0.5. The nonlinear refractive index is $n_2 = 2.2$ x 10-13 m^2/W, and the plot of 20,000 iterations are operated. The system of the fast light generation consist the multi-stage micro ring resonators, where the ring radii are 10, 5 and 10 microns, respectively. The soliton pulse is coupled into the system with $\kappa = 0.25$-0.5.The selected input pulse widths are 50 ns, 50 ps and 50 fs, with wavelength of 1550 nm. After the first micro ring resonator, there is part of the optical power coupled into the second and third ring resonator, respectively. The wave guided loss of 0.5dBmm^{-1} is noted. The simulation results with different input peak powers of 7.5, 12.0 and 20.0 W, with pulse widths of 50 ns, ps, fs, as, and zs are investigated. The simulation results of the output signals at the resonant peak power with 20,000 roundtrips. One set of the simulation results has shown that the clear single attosecond pulse could be filtered by using the simulation parameters as followings: ring radii 5-10 microns, input power 12 W, pulse width 50 fs, coupling coefficient $\kappa = 0.5$. However, all parameters may be changed to investigate more behaviors and characteristics of the devices. The attosecond pulse width of 50 as at FWHM is expanded within 20,000 roundtrips, which the one roundtrip is 2.9 x 10^{-12} sec. The input pulse width of 50 fs is applied into the system. Where the other pulses are interfered and filtered within the device. However, the output peak is amplified by the Kerr nonlinear effect within the ring devices. The resonant peak is obtained by the superposition which is called four-wave mixing type. In practice, the input power is used the commercial laser diode, which is available in the commercial market [47].

4.2 Soliton Pulse Generation

Optical Soliton has been recognized as a nonlinear solitary wave for years [48,49]. Since then, it has been widely investigated in several subjects such as in physics, mathematics and communication, especially, in optical communication. Generally, the common property of a soliton known as self-phase modulation (SPM) and cross phase modulation (XPM) are the challenged behaviors. Furthermore, the non-dispersion behavior of the soliton is the key advantageous. This is capable the use in long-haul communication, where the long distance link without a repeater can be employed. The other interesting soliton behavior is the localization, where the soliton pulse can be trapped and stored within the periodic medium, which is useful in many areas of applications. Generally, the soliton pulse can be recovered, when the balance between dispersion and nonlinear lengths of the soliton pulse exhibits the soliton behavior known as self-phase modulation, it occurs when the matching between the soliton property and localized media is provided. When the generation of the localized soliton pulse is achieved, it is available for applications in many areas of research in science and technology. Recently, the use of a chaotic soliton to form a fast light generation within a tiny device known as a micro ring resonator (waveguide) has been reported by Yupapin et al [50]. They have shown that the large bandwidth can be compressed coherently with a small group velocity. In practice, there are such devices have been fabricated and used [51,52] in various applications.

In this thesis, we show that the large bandwidth of soliton pulse is generated and filtered within the micro ring resonator system. The selected (tuned) pulse is coherently localized and stored within the ring device. In applications, we can use the tuned lsoliton pulses to perform the required applications such as dense wavelength division multiplexing (DWDM) based soliton communication, optical and quantum memory, and multi soliton sources.

An optical soliton is recognized as a powerful laser pulse, which can be used to enlarge the optical bandwidth when propagating within the nonlinear micro ring resonator. Moreover, the soliton self-phase modulation (SPM) keeps the large output gain. When the soliton pulse is introduced into the multi-stage micro an ring resonators as shown in Figure 4.3, the input optical field (E_{in}) is given by equation (4.1).

where A and z are the optical field amplitude and propagation distance, respectively. T is a soliton pulse propagation time, and $L_D = T_0^2 / |\beta_2| i$ is the dispersion length of the soliton pulse. β_2 is propagation constant. This solution describes a pulse that keeps its temporal width invariance as it propagates, and thus is called a temporal soliton. When a soliton peak intensity $\left(\left|\beta_2 / \gamma T_0^2\right|\right)$ is given, then T_o is known. For instance, when the soliton pulse is input into a micro ring resonator at wavelength of 1.55 μm, with a 12 W peak power, then $T_o = 50ns$. This is a pulse of about 2 mm (in z). For the soliton pulse in the micro ring device, a balance should be achieved between the dispersion length (L_D) and the nonlinear length ($L_{NL} = (1/\gamma\phi_{NL})$, where γ and ϕ_{NL} are a coupling loss of the field amplitude and nonlinear phase shift respectively. They are the length scales over which dispersive or nonlinear effects makes the beam becomes wider or narrower. For a soliton pulse, there is a balance between dispersion and nonlinear lengths, hence $L_D = L_{NL}$.

where n_0 and n_2 are the linear and nonlinear refractive indexes, respectively. I and P are the optical intensity and optical power, respectively. The effective mode

core area of the device is given by A_{eff}. For the micro ring and nano ring resonators, the effective mode core areas range from 0.50 to 0.1 μm2 [53].

When a soliton pulse is input and propagated within a micro ring resonator as shown in Figure 4.2: which can be a series micro ring resonators. The resonant output is formed, thus, the normalized output of the light field (E_{out}) can be expressed as

$$\left|\frac{E_{out}}{E_{in}}\right|^2 = (1-\gamma)\left[1-\frac{(1-(1-\gamma)x^2)\kappa}{(1-x\sqrt{1-\gamma}\sqrt{1-\kappa})^2+4x\sqrt{1-\gamma}\sqrt{1-\kappa}\sin^2(\frac{\phi}{2})}\right] \tag{4.4}$$

The close form of equation (4.4) indicates that a ring resonator in the particular case to very similar to a Fabry-Perot cavity, which has an input and output mirror with a field reflectivity, $(1-\kappa)$, and a fully reflecting mirror. Where κ is the coupling coefficient, and $x = \exp(-\alpha L/2)$ represents a roundtrip loss coefficient, $\phi_0 = kLn_0$ and $\phi_{NL} = kLn_2|E_{in}|^2$ are the linear and nonlinear phase shifts respectively, $k = 2\pi/\lambda$ is the wave propagation number in a vacuum. Where L and α are a waveguide length and linear absorption coefficient, respectively. In this work, the iterative method is introduced to obtain the result as shown in equation (4.4), similarly, when the output field is connected and input into the other ring resonators.

After the large bandwidth signals are generated within the first micro ring device, then the filtering device is required to tune the required signals. In order to tune the signals from large bandwidth, we propose to use the add/drop device by using the appropriate parameters. This is given in details as followings. The optical circuit of the add/drop filters can be given by the equations (4.5) and (4.6), where $\beta = kn_{eff}$ is the propagation constant, n_{eff} is the effective refractive index of the waveguide and the circumference of the ring is $L = 2\pi R$, here R is the radius of the ring.

$$\left|\frac{E_t}{E_{in}}\right|^2 = \frac{(1-\kappa_1)-2\sqrt{1-\kappa_1}\cdot\sqrt{1-\kappa_2}e^{-\frac{\alpha}{2}L}\cos(k_nL)+(1-\kappa_2)e^{-\alpha L}}{1+(1-\kappa_1)(1-\kappa_2)e^{-\alpha L}-2\sqrt{1-\kappa_1}\cdot\sqrt{1-\kappa_2}e^{-\frac{\alpha}{2}L}\cos(k_nL)} \tag{4.5}$$

Where the equation (4.6) and the equation (4.5) from the add/drop equation as,

$$\left|\frac{E_d}{E_{in}}\right|^2 = \frac{\kappa_1\kappa_2 e^{-\frac{\alpha}{2}L}}{1+(1-\kappa_1)(1-\kappa_2)e^{-\alpha L}-2\sqrt{1-\kappa_1}\cdot\sqrt{1-\kappa_2}e^{-\frac{\alpha}{2}L}\cos(k_nL)} \tag{4.6}$$

Where E_t and E_d are the throughput and drop port signals, respectively, and $\phi = \beta L$ is the phase constant. The required tunable signals can be managed by using the specific parameters of the add/drop device.

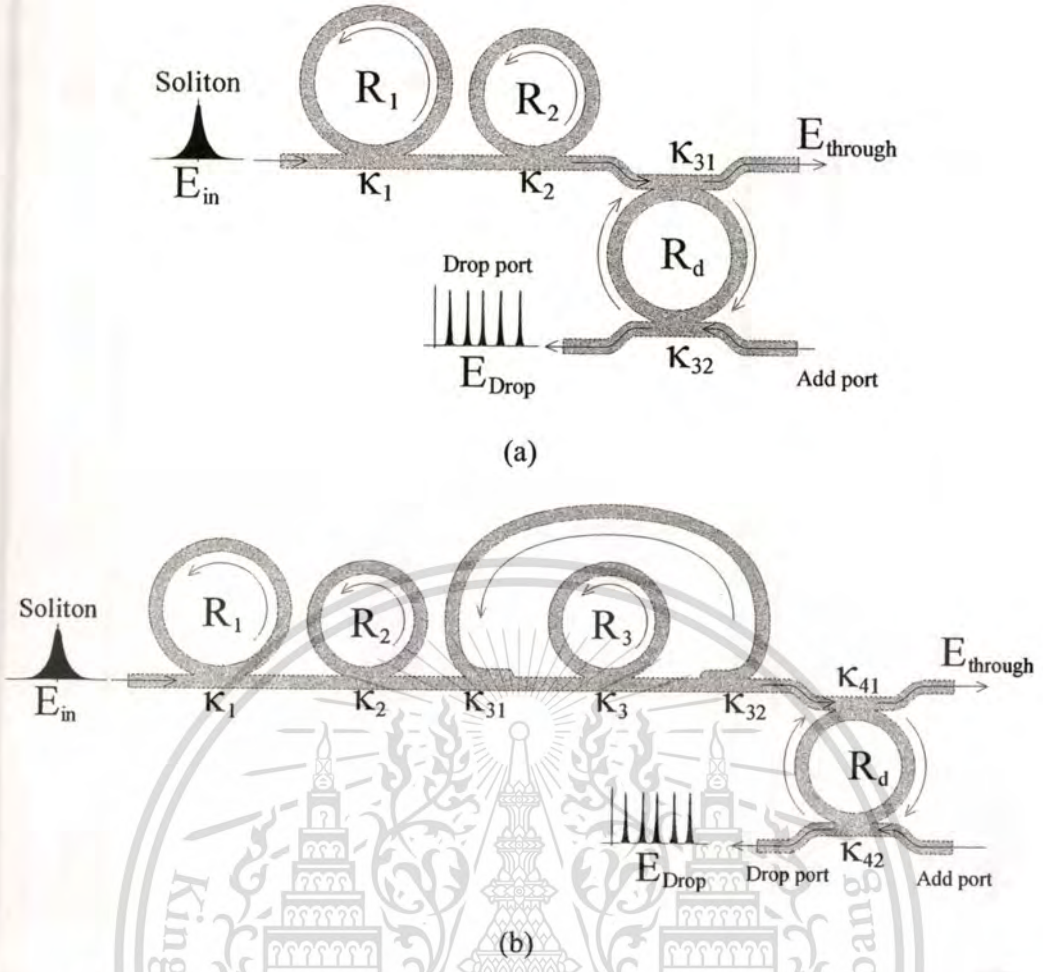

Figure 4.3: Schematic of multi-soliton pulse generation system, where (a) multi-soliton generation, (b) multi-soliton memory, Rs: ring radii, κs: coupling coefficients, κ_{31} and κ_{31} are coupling losses.

4.3 Dark-Bright Optical Solitons

Nonlinear behaviors have shown the potential applications in many research areas, where the interesting concept is that the penalty of nonlinearity becomes benefit [54,55]. They have shown that nonlinear behaviors of light within fiber optic could be used to form the benefits in various research applications. To date, the progress in new linear device technology is quite slow, which may be limited in the near future. Therefore, the trend of new device and technology is become the interesting subject of research today. Nonlinear device is one of the target device and technology that should be encouraged to research for the new era of technology of the world. The interesting results of the nonlinear device that have been reported [56,57], they have shown the interesting and promising result of using the nonlinear device known as a "nano-ring resonator" in various applications. Further, the evidence of such a device using in the laboratory has also been report [58]. The device is fabricated by using the nonlinear material called "InGaAsP/InP", where the nonlinear refractive index is one of the properties of the key phenomenon and good results. To begin this concept, we introduce the device known as a "ring resonator", which is in the circular form or planar

waveguide. Yupapin et al [56] have shown the promising applications when the ring radius is down to micrometer or nanometer. For instance, the ultra fast switching can be easily generated by using a remarkably simple arrangement, where the achievement of the switching time of attosecond and beyond is confirmed. The most interesting results is seen when light pulse can be slow down, stopped and stored within the nonlinear nano-waveguide, where the signal amplification within the tiny device has shown the great successful.

Dark and bright soliton behaviors have been widely investigated in different forms [60,61]. The use of soliton, i.e. bright soliton in long distance communication link has been implemented for nearly two decades, however, the interesting works using bright solitton in communication remain, whereas the use a soliton pulse within a micro ring resonator for communication security has been studied [62]. Dark soliton is one of the soliton properties, whereas the soliton amplitude is vanished or minimized during the propagation in media, therefore, the dark soliton detection is difficult. The investigation of dark soliton behaviors has been reported [63], where one point of them has shown the interesting results, where the dark soliton can be stabilized [64] and converted into bright soliton [65] and finally detected. This means that we can use the dark soliton penalty due to the low level of the peak power to be the benefit, where the promising idea is that a dark soliton can be performed the communication transmission carrier where the recovery can be retrieved by the dark-bright soliton conversion. Actually, we are looking for the simple technique that can be employed to detect the dark soliton. Yupapin and Suwancharoen have reported [66] the interesting results of light pulse propagating within a nonlinear micro ring device, where the transfer function of the output at the resonant condition is derived and used. They found that the broad spectrum of light pulse can be transformed to the discrete pulses. In this letter, we have shown that after the clean dark soliton is input and chopped to be the noisy signals for security purpose within the nonlinear ring resonator system, which can be transmitted into the transmission link safely. The required users can retrieve the original signal via an add/drop filter, where they can chose to retrieve in either bright or dark soliton pulses. However, the device parameters are the given keys for the end users, where they can use to form the device that can be used to retrieve the signals in the link or network. The conversion signal amplification is also interesting technique. We find that the significant amplified signals can be achieved.

An optical soliton is recognized as a powerful laser pulse, which can be used to enlarge the optical bandwidth when propagating within the nonlinear micro ring resonator. Moreover, the superposition of self-phase modulation soliton pulses can keep the large output power. Initially, the optimum energy is coupled into the waveguide by a lager effective core area device, i.e. micro ring resonator. Then the smaller one is connected to transfer the soliton power, however, the optical loss is involved in the transferring link. The filtering characteristic of the optical signal is presented within an add/drop filter, where the suitable parameters can be controlled to obtain the required output energy. To obtain the required soliton power after propagating within the ring resonator, the suitable coupling power into the device is required, i.e. coupling coefficient (κ), whereas the interference signal is a minor effect compared to the loss associated to the direct passing through.

We are looking for a stationary dark soliton pulse, which is introduced into the multi-stage micro ring resonators as shown in Figure 4.4 , the input optical field (E_{in}) of the dark soliton pulse input is given by

$$E_{in}(t) = A\tanh\left[\frac{T}{T_0}\right]\exp\left[\left(\frac{z}{2L_D}\right) - i\omega_0 t\right] \quad (4.7)$$

Where A and z are the optical field amplitude and propagation distance, respectively. T is a soliton pulse propagation time in a frame moving at the group velocity, $T = t\text{-}\beta_1 * z$, where β_1 and β_2 are the coefficients of the linear and second order terms of Taylor expansion of the propagation constant. $L_D = T_0^2/|\beta_2|$ is the dispersion length of the soliton pulse. To in equation is a soliton pulse propagation time at initial input. Where t is the soliton phase shift time, and he frequency shift of the soliton is ω_0. This solution describes a pulse that keeps its temporal width invariance as it propagates, and thus is called a temporal soliton. When a soliton peak intensity $\left(|\beta_2/\Gamma T_0^2|\right)$ is given, then T_o is known. For the soliton pulse in the micro ring device, a balance should be achieved between the dispersion length (L_D) and the nonlinear length ($L_{NL} = (1/\Gamma\phi_{NL})$, where $\Gamma = n_2 * k_0$, is the length scale over which dispersive or nonlinear effects makes the beam becomes wider or narrower. For a soliton pulse, there is a balance between dispersion and nonlinear lengths, hence $L_D = L_{NL}$.

When light propagates within the nonlinear material (medium), the refractive index (n) of light within the medium is given by equation (4.2).

where n_0 and n_2 are the linear and nonlinear refractive indexes, respectively. I and P are the optical intensity and optical power, respectively. The effective mode core area of the device is given by A_{eff}. For the micro ring and nano ring resonators, the effective mode core areas range from 0.50 to 0.10 μm^2 [56].

When a soliton pulse is input and propagated within a micro ring resonator as shown in Figure. 1, which consists of a series micro ring resonators. The resonant output is formed, thus, the normalized output of the light field is the ratio between the output and input fields ($E_{out}(t)$ and $E_{in}(t)$) in each roundtrip, which is given by equation (4.4).

The close form of equation (4.4) indicates that a ring resonator in the particular case is very similar to a Fabry-Perot cavity, which has an input and output mirror with a field reflectivity, ($1\text{-}\kappa$), and a fully reflecting mirror. κ is the coupling coefficient, and $x = \exp(-\alpha L/2)$ represents a roundtrip loss coefficient, $\phi_0 = kLn_0$ and $\phi_{NL} = kLn_2|E_{in}|^2$ are the linear and nonlinear phase shifts, $k = 2\pi/\lambda$ is the wave propagation number in a vacuum. Where L and α are a waveguide length and linear absorption coefficient, respectively. In this work, the iterative method is introduced to obtain the results as shown in equation (4.4), similarly, when the output field is connected and input into the other ring resonators.

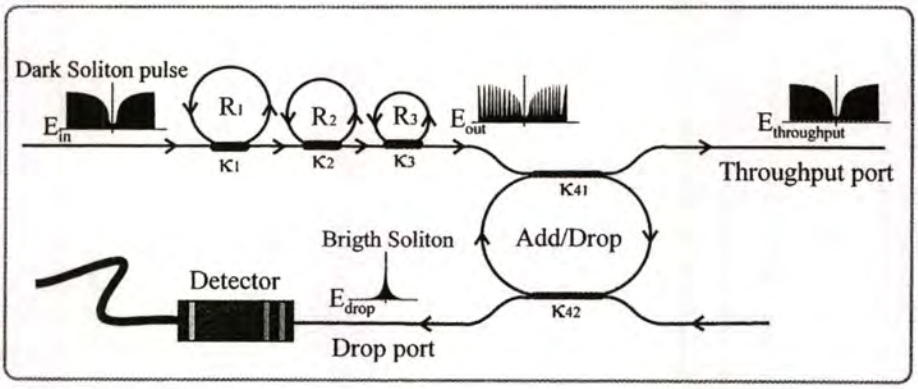

Figure 4.4: A schematic of a dark-bright soliton conversion system, where Rs: ring radii, κs: coupling coefficients, κ_{41} and κ_{42} are the add/drop coupling coefficients.

After the signals are multiplexed with the generated chaotic noise, then the chaotic cancellation is required by the individual user. To retrieve the signals from the chaotic noise, we propose to use the add/drop device with the appropriate parameters. This is given in details as followings. The optical circuits of ring-resonator add/drop filters for the throughput and drop port can be given by equations (4.5) and (4.6), respectively [66].

where E_t and E_d represents the optical fields of the throughput and drop ports respectively. $\beta = kn_{eff}$ is the propagation constant, n_{eff} is the effective refractive index of the waveguide and the circumference of the ring is $L = 2\pi R$, here R is the radius of the ring. In the following, new parameters will be used for simplification: $\phi = \beta L$ is the phase constant. The chaotic noise cancellation can be managed by using the specific parameters of the add/drop device, which the required signals can be retrieved by the specific users. $\kappa_1$and κ_2 are coupling coefficient of add/drop filters, $k_n = 2\pi / \lambda$ is the wave propagation number for in a vacuum, and where the waveguide (ring resonator) loss is $\alpha = 0.5$ dBmm^{-1}. The fractional coupler intensity loss is $\gamma = 0.1$. In the case of add/drop device, the nonlinear refractive index is neglected.

4.4 Conclusion

In this chapter, the interesting optical system of the dark-bright optical soliton using a micro ring resonators an optical add/drop multiplexer that can be integrated into single system. The large bandwidth signal is generated by using a soliton pulse propagating in Kerr-type nonlinear medium. Results shown that the generation of the multi-soliton pulse within the micro-ring resonator.

CHAPTER 5
SOLITON PULSE GENERATION IN MICRORING RESONATORS FOR DWDM

Optical Soliton has been recognized as a nonlinear solitary wave for years. Since then, it has been widely investigated in several subjects such as in physics, mathematics and communication, especially, in optical communication. Generally, the common property of a soliton known as self-phase modulation (SPM) and cross phase modulation (XPM) are the challenged behaviors. Furthermore, the non-dispersion behavior of the soliton is the key advantageous. This is capable the use in long-haul communication, where the long distance link without a repeater can be employed. The other interesting soliton behavior is the localization, where the soliton pulse can be trapped and stored within the periodic medium, which is useful in many areas of applications. Generally, the soliton pulse can be recovered, when the balance between dispersion and nonlinear lengths of the soliton pulse exhibits the soliton behavior known as self-phase modulation, it occurs when the matching between the soliton property and localized media is provided. When the generation of the localized soliton pulse is achieved, it is available for applications in many areas of research in science and technology. Recently, the use of a chaotic soliton to form a fast light generation within a tiny device known as a micro ring resonator (waveguide). They have shown that the large bandwidth can be compressed coherently with a small group velocity. In practice, there are such devices have been fabricated and used in various applications.

In this thesis, we show that the large bandwidth of soliton pulse is generated and filtered within the micro ring resonator system. The selected (tuned) pulse is coherently localized and stored within the ring device. In applications, we can use the tuned lsoliton pulses to perform the required applications such as dense wavelength division multiplexing (DWDM) based soliton communication, optical and quantum memory, and multi soliton sources.

5.1 Optical Filters

5.1.1 Frequency Filter

In this section, the key point is that the two different frequencies can be simultaneously filtered from the broad spectrum, where the up-down-link converters can be simultaneously operated within a single system. The proposed system of the simultaneous fast and slow light generation is as shown in Figure 4.1. The single mode soliton pulse is become many modes (noisy signals) after circulating within the first micro ring device due to the nonlinear Kerr effects of light within the micro ring resonator. The chaotic filtering characteristics of the signals are formed by the other ring resonators within the system. By using the material parameters of *InGaAsP/InP*, the specified frequency bands can be obtained by using the appropriate ring parameters, finally, we end up with the following details. The soliton waveform with the center frequency at 2 GHz is input into the first micro ring resonator (R_1). The optical power is fixed to 550 mW, $f_0 = 2$ GHz, $n_0 = 3.34$, $n_2 = 2.2 \times 10^{-17}$ m^2W^{-1}, $A_{eff} = 0.50$ μm^2, $\alpha = 0.5$ $dBmm^{-1}$, $\gamma = 0.1$, with 20,000 roundtrips. The chaotic signals are generated within the

first ring (R_1), where the broad frequency band is obtained within the ring R_2. The clearer filtering signals are seen in ring R_3 and R_4.

Figure 5.1 shows graph of the simultaneous fast and slow light generation for two different frequency bands. Where the parameters are R_1 = 10 μm, κ_1 = 0.9713, R_2 = 10 μm, κ_2 = 0.9718, R_3 = 10 μm, κ_3 = 0.9718, R_4 = 15 μm, $\kappa 4$ = 0.9728. Two sigle frequency bands are filtered as shown shown in Figure 5.2 and 5.3, respectively. Figure 5.2 shows graph of fast and slow light generation that can be operated for down-link converter. Where the parameters used are R_1 = 10 μm, κ_1 = 0.9713, R_2 = 10 μm, κ_2 = 0.9718, R_3 = 10 μm, κ_3 = 0.9718, R_4 = 15 μm, κ_4 = 0.9728. Figure 5.3 shows graph of fast and slow light generation for up-link converter. When the parameters used are R_1 = 10 μm, κ_1 = 0.9713, R_2 = 10 μm, κ_2 = 0.973, R_3 = 10 μm, κ_3 = 0.9732, R_4 = 15 μm, κ_4 = 0.9777. In application, the upstream and downstream communication information can be linked via a single system of devices as shown in Figure 4.1, for the up-down-link converters. In principle, the communication signals are formed by the signal interchanging devices known as Electrical to Optical (E/O) and Optical to Electrical (O/E) converters. In the system the up-link and down-link frequency bands can be simultaneously generated and filtered, therefore, the next step is that the specified frequency band will be filtered to form the required link converters. By using the proposed system, the wide range of the spread frequency spectrum can also be generated and available.

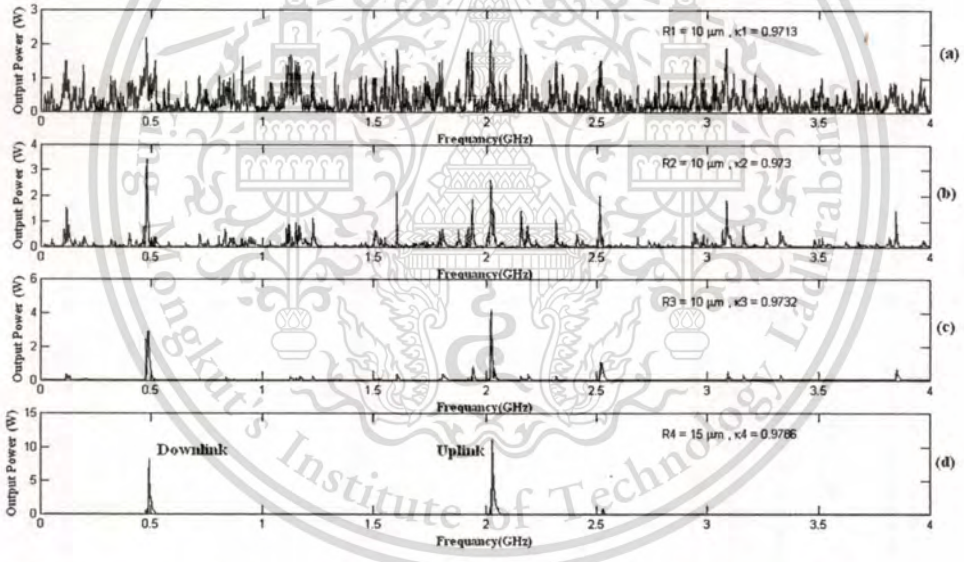

Figure 5.1: Graph of simultaneous fast and slow light generation for up-down-link converters, (a) noisy chaotic signals, (b) a broad frequency spectrum, (c) and (d) the clear filtering signals.

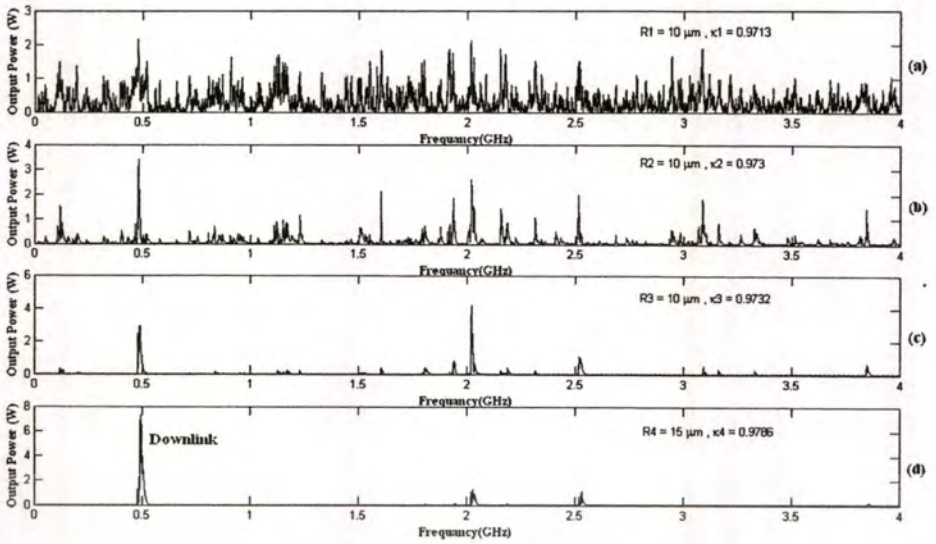

Figure 5.2: Graph of fast and slow light generation for down-link converter, (a) noisy chaotic signals, (b) broad frequency bands, (c) and (d) the specific filtering signals (500MHz).

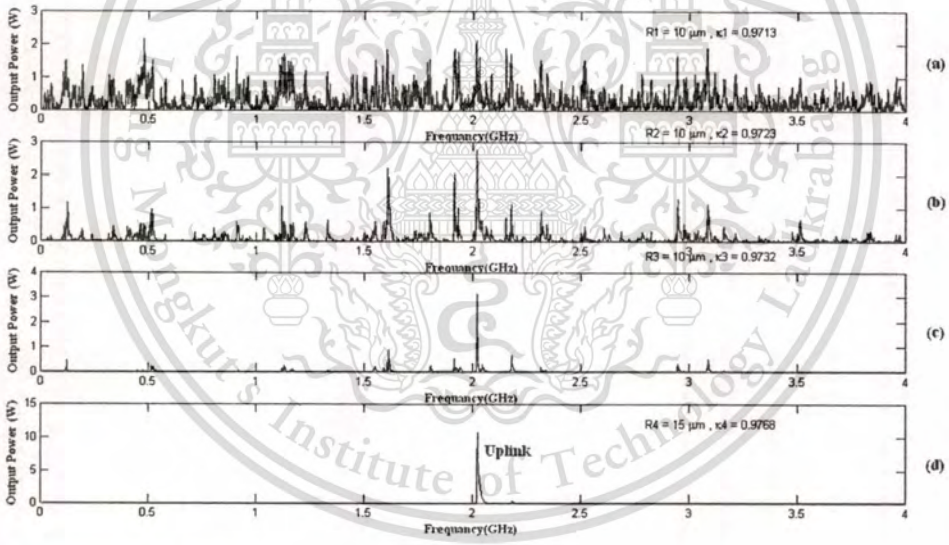

Figure 5.3: Graph of fast and slow light generation for up-link converter, (a) noisy chaotic signals, (b) broad frequency bands, (c) and (d) the specific filtering signals (2GHz).

5.1.2 Wavelength Filter

The remarkably simple system of the wavelength generation and filtering using a serial micro ring resonator is as shown in Figure 4.2 When a soliton pulse is input into the nonlinear Kerr effects medium (i.e. a nonlinear micro ring resonator), the nonlinear behavior known as chaos is introduced as shown in Figure 5.4. For instance, to make the system associate with the practical device , the selected parameters of the system are fixed to λ_0 = 1.55 μm, n_0 = 3.34 (*InGaAsP/InP*), A_{eff} = 0.50 μm^2, α = 0.02 $dBkm^{-1}$, γ = 0.1, and R_1 = 20 μm. The coupling coefficient of the micro ring resonator is fixed at κ = 0.5-0.9. The nonlinear refractive index is $n_2 = 2.2 \times 10^{-17}$ m^2/W. In this section, the system of the third harmonic generation consist the multi-stage micro ring resonators, where the ring radii are selected between 5 and 32 μm. The soliton pulse is coupled into the system with optical power of 1 W, coupling constants (kappa), κ = 0.5-0.9.The selected input pulse widths are 50 ns, 50 ps, 50 fs and 50 as, with the centre wavelength at 1550 nm. After the first micro ring resonator, the optical power is coupled into the second and third ring resonator, respectively. In this case, the wave guided loss used is $0.5dBmm^{-1}$. In Figure 5.6, when the input soliton with pulse width of 50 ns is input into the system, the chaotic behaviors are occurred within the micro ring resonators R_1 and R_2, when the ring radii are 20 and 5 μm, respectively.

Generally, The required filtering signals can be obtained by using the appropriate ring parameters. For instance, the UV wavelength is obtained within the last micro ring, i.e. R_3, with the ring radius of 28 μm. The coupling constants used are 0.9 and 0.5 for κ_1 and κ_2=κ_3, respectively. Similarly, when the other soliton pulses with different pulse widths is input into the same system. The comparison of the filtering signals of the different input soliton pulses are shown in Figure 5.5. In principle, the generation pulse width beyond the attosecond input pulse, i.e. zeptosecond, is also plausible. In applications, the exact roundtrips time at the resonant peak power can be controlled and selected by the optical soliton input power and ring parameters, which can be selected the required filtering signals.

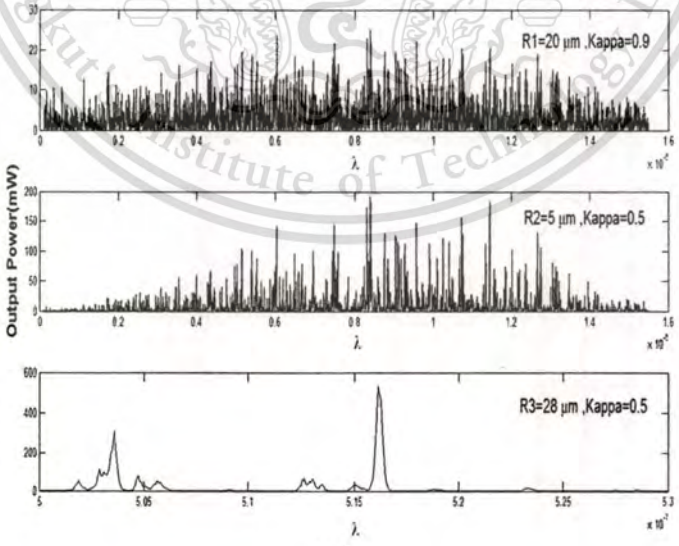

(a)

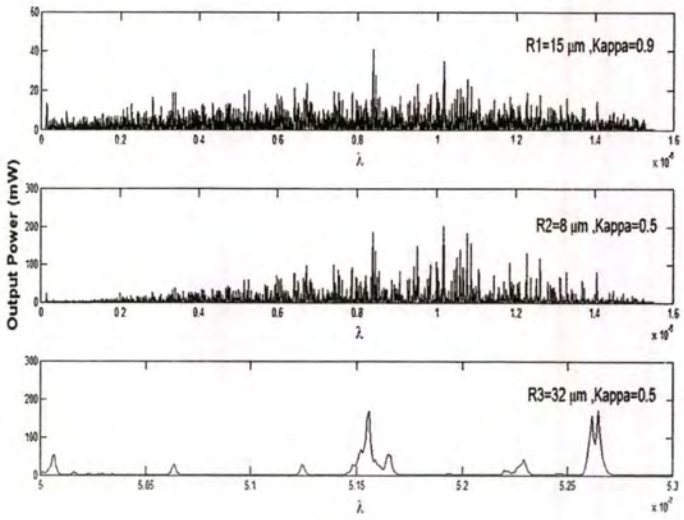

(b)

Figure 5.4: Results of the broad spectrum of the filtering signals, where the input soliton pulses are (a) 50 ns input, R_1=20μm, R_2=5μm, R_3=28μm, and (b) 50 as input, R_1=15μm, R_2=5μm, R_3=32 μm.

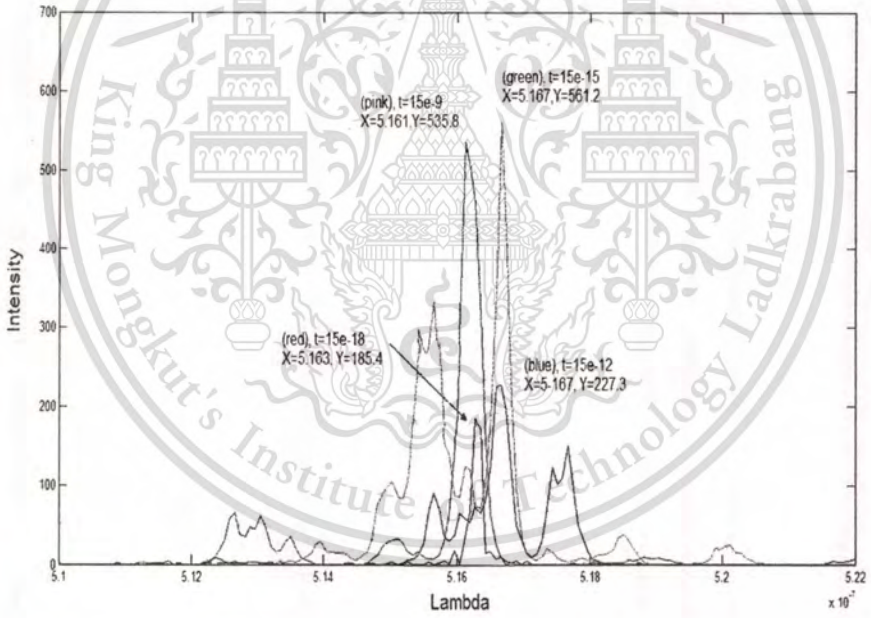

Figure 5.5: Results of the selected outputs after the wavelength filter in all cases.

5.1.3 Ultra Fast Filter

The simple system of the fast light generation and filtering using a serial micro ring resonator is a similar system as shown in Figure 4.1 When a soliton pulse is input into the nonlinear Kerr effects medium, the nonlinear behavior of light traveling in a micro ring resonator is introduced. The parameters of the system are fixed

to $\lambda_0 = 1.55$ μm, $n_0 = 3.34$ (*InGaAsP/InP*), $A_{eff} = 0.50$ μm^2, $\alpha = 0.02$ dBkm^{-1}, $\gamma = 0.1$, and $R_1 = 10$ μm. The coupling coefficient of the micro ring resonator is fixed at $\kappa = 0.25$-0.5. The nonlinear refractive index is $n_2 = 2.2 \times 10^{-13}$ m^2/W, and the plot of 20,000 iterations are operated. The system of the fast light generation consist the multi-stage micro ring resonators, where the ring radii are 10, 5 and 10 microns, respectively. The soliton pulse is coupled into the system with $\kappa = 0.25$-0.5.The selected input pulse widths are 50 ns, 50 ps and 50 fs, with wavelength of 1550 nm. After the first micro ring resonator, there is part of the optical power coupled into the second and third ring resonator, respectively. The wave guided loss of 0.5dBmm^{-1} is noted. The simulation results with different input peak powers of 7.5, 12.0 and 20.0 W, with pulse widths of 50 ns, ps, fs, as, and zs are investigated. The simulation results of the output signals at the resonant peak power with 20,000 roundtrips are shown in Figure 5.6 - 5.8. One set of the simulation results has shown that the clear single attosecond pulse could be filtered as shown in Figure 5.7(d), by using the simulation parameters as followings: ring radii 5-10 microns, input power 12 W, pulse width 50 fs, coupling coefficient $\kappa = 0.5$. However, all parameters may be changed to investigate more behaviors and characteristics of the devices. In Figure 5.8, the attosecond pulse width of 50 as at FWHM is expanded within 20,000 roundtrips, which the one roundtrip is 2.9×10^{-12} sec. The input pulse width of 50 fs is applied into the system. Where the other pulses are interfered and filtered within the device. However, the output peak is amplified by the Kerr nonlinear effect within the ring devices. The resonant peak is obtained by the superposition which is called four-wave mixing type. In practice, the input power is used the commercial laser diode, which is available in the commercial market .

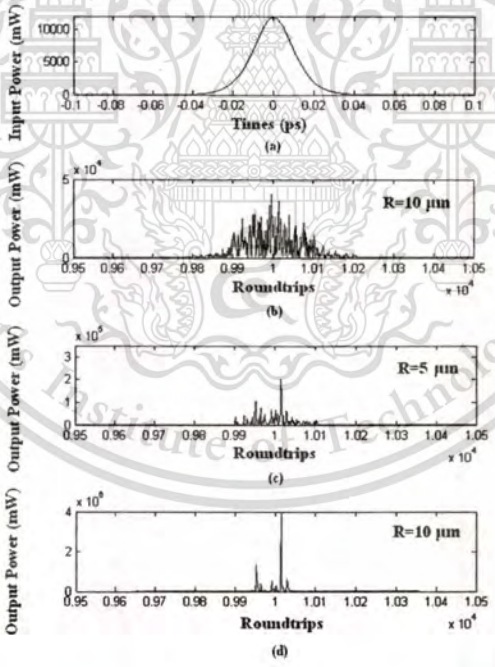

Figure 5.6: Results of fast light filter with 50 ps (a) input pulse(a), coupling constant $\kappa = 0.5$, where the ring radii are 10 μm (b), 5 μm (c) and 10 μm (d).

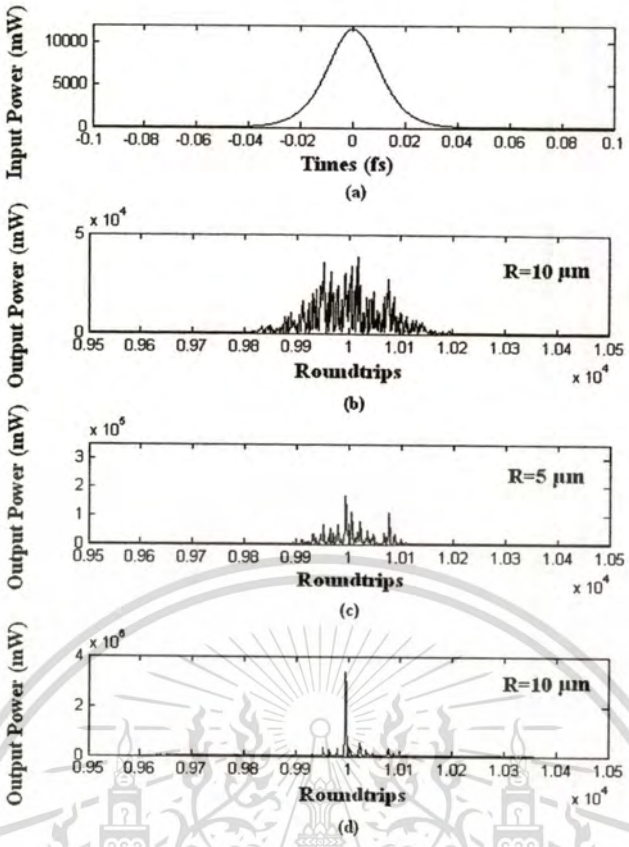

Figure 5.7: Results of fast light filter with 50 fs (a) input pulse (a), coupling constant $\kappa = 0.5$, where the ring radii are 10 μm (b), 5 μm (c) and 10 μm (d).

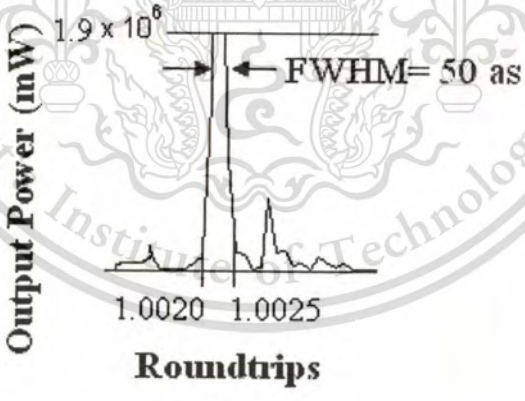

Figure 5.8: Shows the pulse width expansion of the output pulse in (d) with the raction of time of 10^{-3} of the input power.

5.2 Soliton Pulse Generation

In operation, the large bandwidth signals can be generated within the micro ring device by using a soliton pulse input into the nonlinear micro ring resonator. The schematic diagram of the proposed system is as shown in Figure 4.3. A soliton pulse with 20 ns pulse width, peak power at 500 mW is input into the system. The suitable ring parameters are used, for instance, ring radii R_1= 10 μm, R_2= 5 μm, and R_d= 200 μm. In order to make the system associate with the practical device, the selected parameters of the system are fixed to λ_0 = 1.55 μm, n_0 = 3.34 (*InGaAsP/InP*), A_{eff}= 0.25 μm2 for all micro ring resonators, α = 0.5 dBmm^{-1}, γ = 0.1. The coupling coefficient (kappa, κ) of the micro ring resonator ranged from 0.50 to 0.975. The nonlinear refractive index is $n_2 = 2.2 \times 10^{-17}$ m^2/W. In this case, the wave guided loss used is 0.5dBmm^{-1}. The signal is chopped (sliced) into a smaller signal spreading over the spectrum as shown in Figure 5.9 (b), which is shown that the large bandwidth (continuous variable) signal is formed within the first ring device. The compress bandwidth with smaller group velocity is obtained within the ring R_2, i.e. filtering signals. The localized soliton concept is formed, when the resonant soliton pulses is seen as shown in Figure 5.9 (d). Since, we have found that the tuned light pulse can be obtained by connecting the add/drop device into the system (i.e. R_2). However, there are two types of soliton pulses, i.e. temporal and spatial solitons. In Figure 5.10, results of the multi-soliton pulse generation, where (a) an input soliton, (b) large bandwidth signals, (c) temporal solitons, (d) spatial solitons. The free spectrum range obtained is 600 pm, and the FWHM of the pulse is 10 pm. The remaining power is 30 mW, which is capable to use in communication networks.

Furthermore, the localized soliton pulses can be stored within the micro ring device as shown in Figure 4.3 (b). In Figure 5.11, results obtained have shown that the multi-soliton pulses can be stored within the device (ring R_3), where the ring radii are R_1= 10 μm, R_2=R_3= 4 μm, and R_d= 200 μm. Results of the multi-soliton pulse generation are ; (a) large bandwidth signals, (b) and (c) temporal solitons, (d) localized solitons and (e) the localized spatial solitons. The amplified optical power is available to perform the transmission link. The tunable spatial solitons are obtained by using the add/drop multiplexer, which means that multi-so;litons can be stored within the ring R_3, whereas the memory time up to 1.4 ns is achieved. The power distribution can be performed via the add/drop filter, radius R_d as shown in Figure 5.11 (e).

The key advantage of the proposed system is the multi-soliton pulses, which is available for high performance network. Since, a soliton communication has been recognized as a good candidate for long distance communication, therefore, the increasing in more soliton channels (wavelengths) is interesting. The increasing in communication capacity is obtained by using more available channels and large bandwidth. A simple system of large bandwidth generation is as shown in Figure 5.12 (a), where the system of the network distribution is shown in Figure 5.12 (b). After the multi-soliton pulses are generated, then transmitted into the networks. The increasing in communication capacity is provided by the increasing in soliton pulses (λ_i), which is formed by the spatial soliton. Furthermore, the communication security is formed by using the temporal soliton, where the quantum codes (qubits) are performed by the individual user in the network. Finally, the high capacity and secured signals can be transmitted and retrieved via the quantum network via the add/drop ports. The required signals can be filtered and retrieved, and the quantum codes can be formed between Alice and Bob.

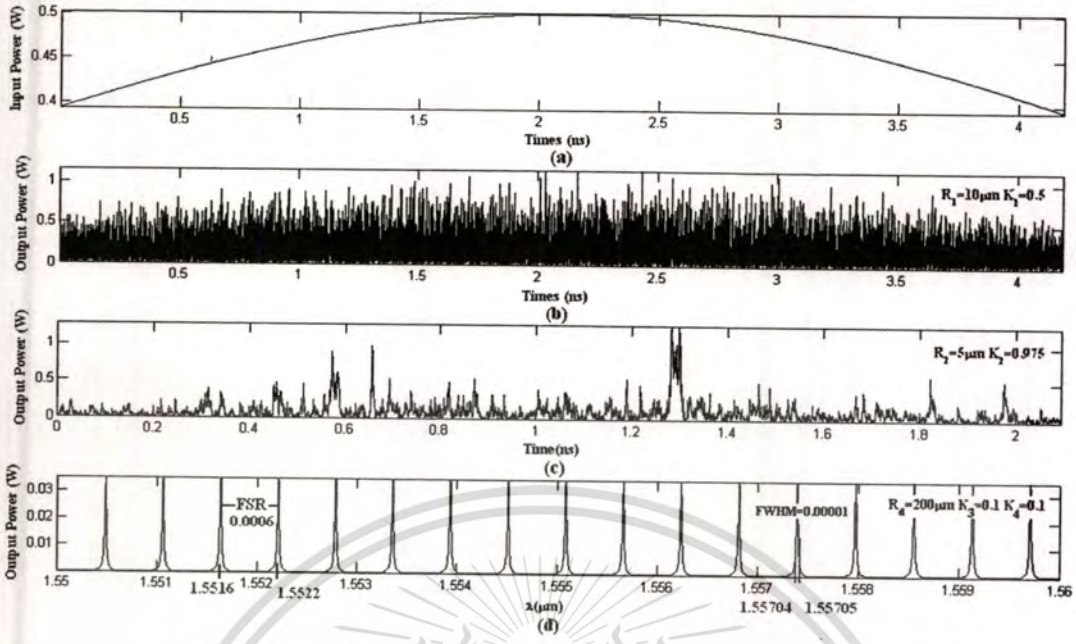

Figure 5.9: Results of the multi-soliton pulse generation, where (a) input soliton, (b) large bandwidth signals, (c) temporal soliton, (d) spatial soliton. The free spectrum range is 600 pm, and the FWHM of the pulse is 10 pm.

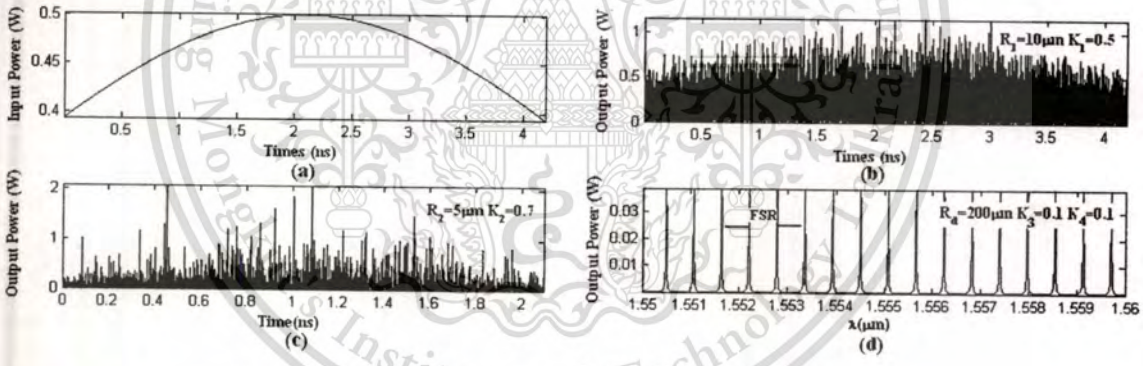

Figure 5.10: Results of temporal(c) and spatial (d) soliton pulses, where the free spectrum range and the pulse FWHM are 600 and 10 pm respectively.

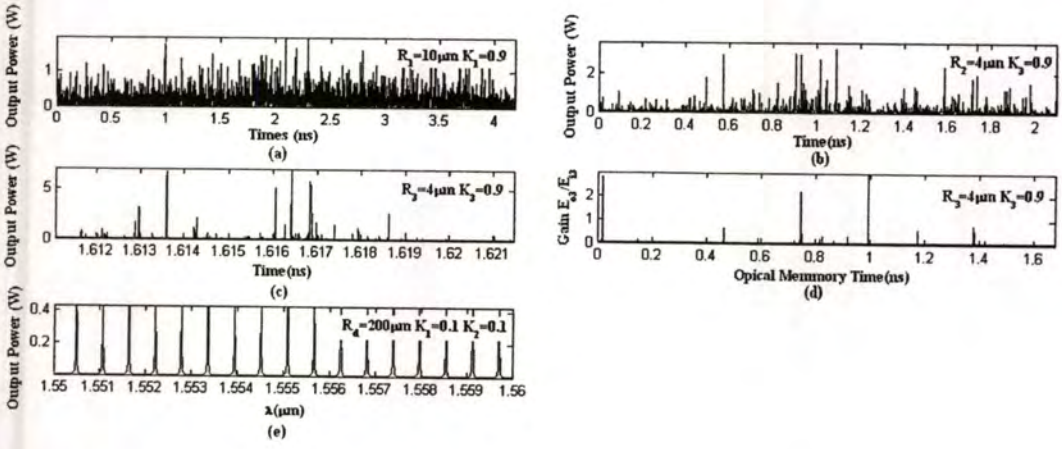

Figure 5.11: Results of the multi-soliton pulse generation using a schematic in Figure 4.3(b), where (a) the large bandwidth signals, (b) and (c) temporal solitons, (d) the localized temporal solitons and (e) the localized spatial soliton.

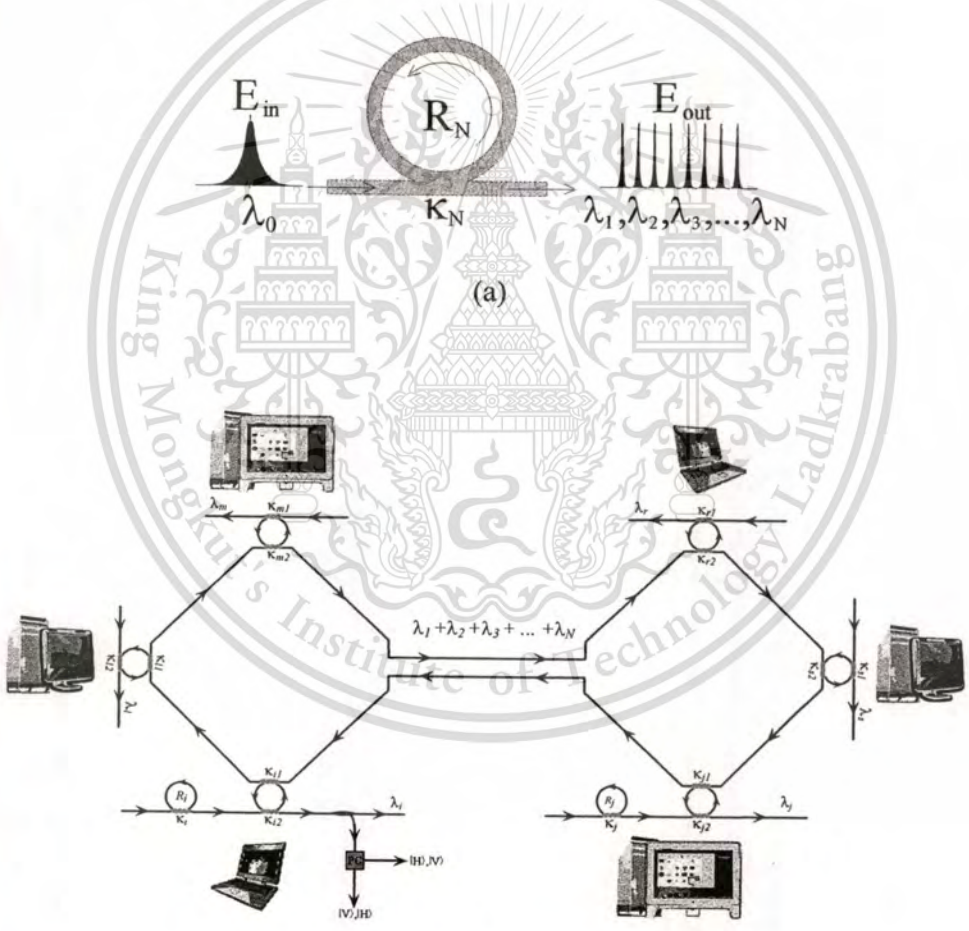

Figure 5.12: Schematic of a large bandwidth signal generation system (a), and (b) a schematic of a wavelength router and network system, where Rs: ring radii and κs, κs_1, κs_2 are the coupling coefficients.

5.3 Dark-Bright Optical Solitons

In operation, a dark soliton pulse with 50 ns pulse width, the maximum power of 0.65 W is input into the dark-bright solitons conversion system as shown in Figure 4.4. The suitable ring parameters are used, for instance, ring radii R_1= 10.0 μm, R_2= 7.0 μm, and R_3= 5.0 μm. In order to make the system associate with the practical device, the selected parameters of the system are fixed to λ_0 = 1.55 μm, n_0 = 3.34 (*InGaAsP/InP*). The effective core areas are A_{eff} = 0.50, 0.25 μm2 and 0.10 μm^2 for a micro ring and nano ring resonator, respectively. The waveguide and the coupling loses are α = 0.5 $dBmm^{-1}$, γ = 0.1, respectively, and the coupling coefficients (kappa, κ) of the micro ring resonator are ranged from 0.05 to 0.90. However, more parameters are used as shown in the figures. The nonlinear refractive index is n_2=2.2 x 10^{-13} m^2/W. In this case, the wave guided loss used is 0.5$dBmm^{-1}$.The input dark soliton pulse is chopped (sliced) into the smaller signals as shown in Figure 5.13(a). Figures 5.13(b) and 5.13(c) are the output signals of the filtering signals within the rings R_2 and R_3. We find that the output signals from R_3 are smaller than from R_1, which is more difficult to detect when it is used in the link. In fact, the multi-stage ring system is proposed due to the different core effective areas of the rings in the system, where the effective areas can be transferred form 0.50 μm^2 to 0.10 μm^2 with some losses. The soliton signals in R_3 is entered in the add/drop filter, where the dark-bright solitons conversion can be performed by using Eqs. (4.5) and (4.6). Results obtained when a dark soliton pulse is input into a micro and nano ring resonator system as shown in Figs. 5.15 and 5.16. The parameters used are the same as in Figure 5.14, where the only change is the add/drop filter parameters. The add/drop filter is formed by two couplers and a ring radius (R_d) of 10 μm, the coupling constants (κ_{11} and κ_{12}) are the same values (0.50). When the add/drop filter is connected to the third ring (R_3), the dark-bright solitons conversion are achieved and seen. The bright soliton and dark solitons are detected by the through (throughput) and drop ports as shown in Figure 4.4, respectively.

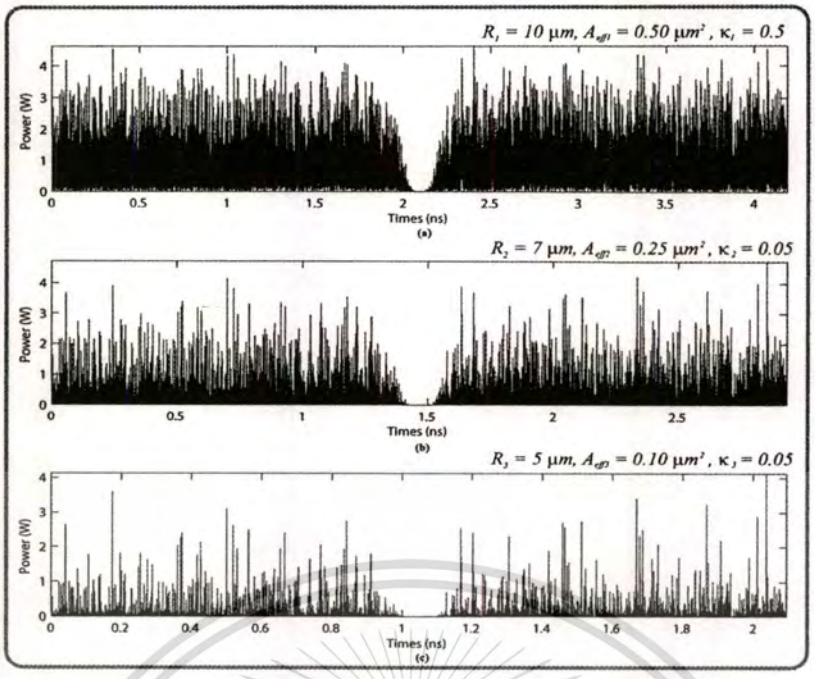

Figure 5.13: Results of the soliton signals within the ring resonator system, where (a) in ring R_1, (b) in ring R_2 and (c) in ring R_3.

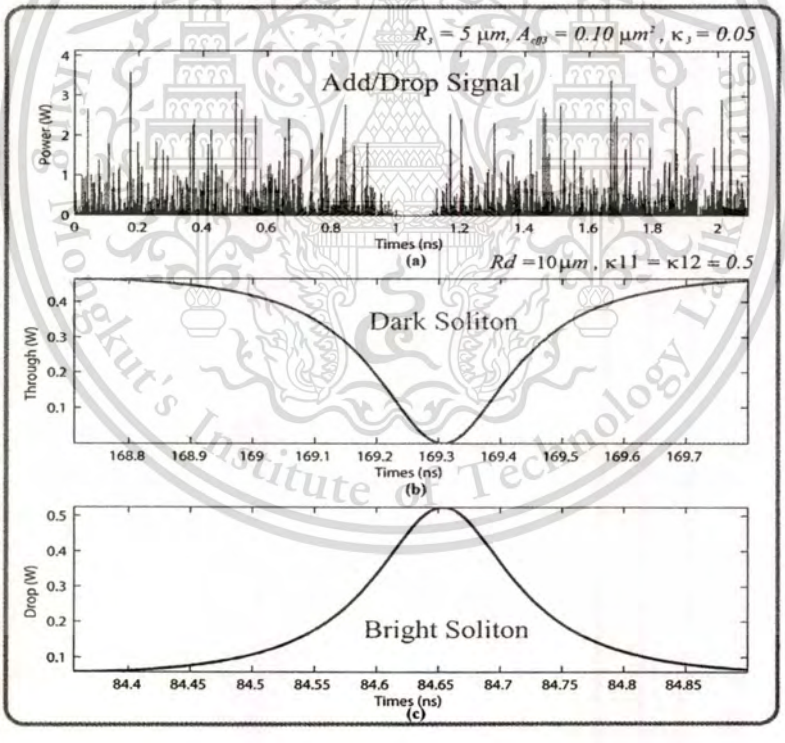

Figure 5.14: Results of the optical solitons, where (a) the signals in R_3, (b) a dark soliton and (c) a bright soliton. The input dark soliton power is 0.65 W, κ_1 = 0.5, R_d= 10 μm.

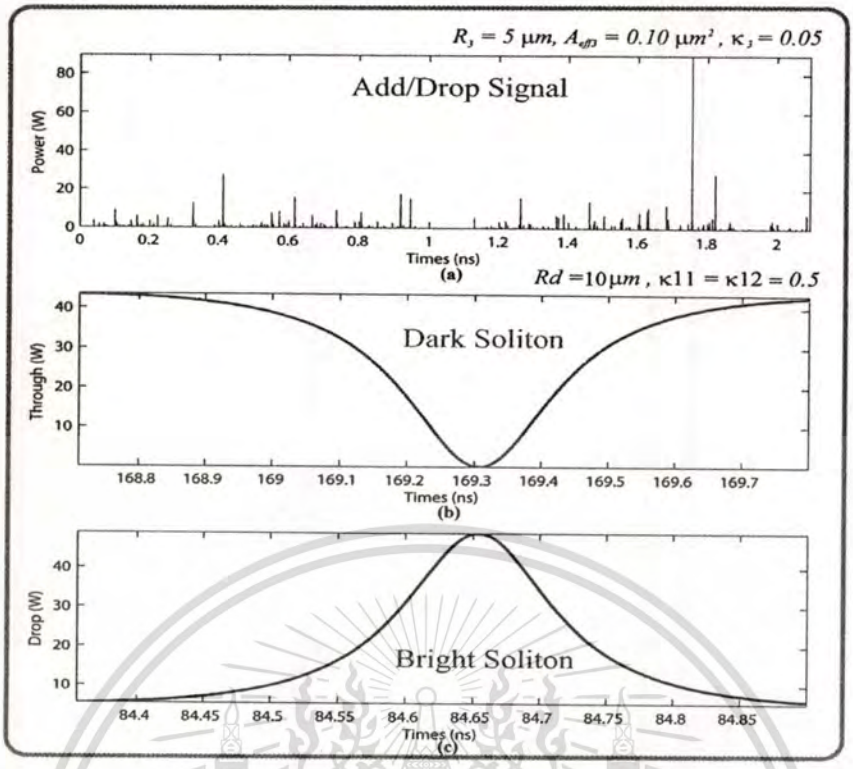

Figure 5.15: Results of the optical solitons, where (a) the signals in R_3, (b) a dark soliton and (c) a bright soliton. The input dark soliton power is 0.65 W, κ_1 = 0.9, R_d= 10 μm.

The dark-bright signal amplification system is as shown in Figure 5.16. Firstly, when the bright soliton system is operated, the large bandwidth within the micro ring device can be generated by using a soliton pulse input into the nonlinear micro ring resonator. Similarly, the input soliton pulse is chopped (sliced) into a smaller signal spreading over the spectrum as shown in Figure 5.17, which is shown that the large bandwidth signal is generated within the first ring device. A soliton pulse with 50 ns pulse width, maximum power at 0.65 W is input into the system. Results obtained when a bright soliton pulse is input into the ring resonator system, whereas the parameters used are R_1= 10 μm, A_{eff1} = 0.50 μm^2, R_2= 7 μm, A_{eff2} = 0.25 μm^2, R_3= 5 μm, A_{eff3} = 0.10 μm^2 and κ_1 = 0.2 and $\kappa_2 = \kappa_3$ = 0.05. The continuous spectra output with 25 times larger than the input is obtained and seen in Figure 5.17(c). Secondly, a soliton pulse is input into a micro ring resonator system for within NRR, where the parameters used are R_1= 10 μm, A_{eff1} = 0.50 μm^2, R_2= 7 μm, A_{eff2} = 0.25 μm^2, R_3= 5 μm, A^{eff3} = 0.10 μm^2 and κ_1 = 0.2 and $\kappa_2 = \kappa_3$= 0.05.A dark soliton pulse is chopped (sliced) into the smaller signals as shown in Figure 5.18(a). Figures 5.18(b) and 5.18(c) are the output signals of the filtering signals within the rings R_2 and R_3. Results obtained when a dark soliton pulse is input into a micro and nano ring resonator system as shown in Figure 5.16(a). The continuous spectra output with 25 times larger than the input is obtained and seen in Figure 5.17(b). The coupling coefficients are given as shown in the figures.

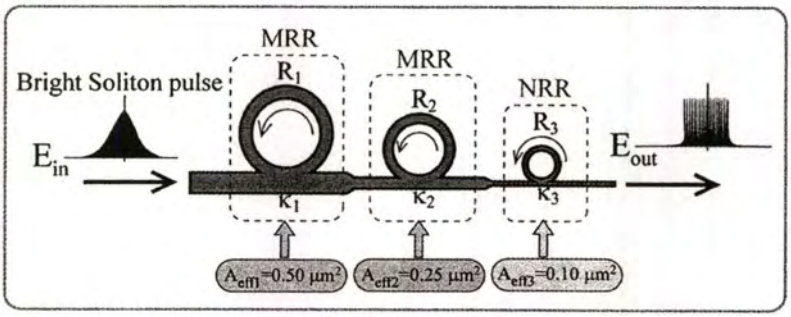

Amplified bright soliton within NRR.

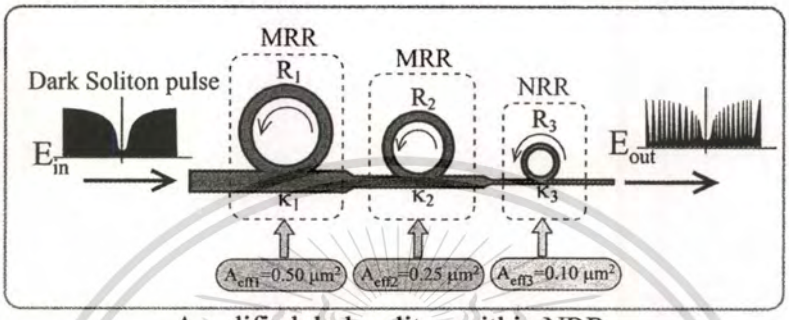

Amplified dark soliton within NRR.

Figure 5.16: A schematic of the amplified dark-bright soliton conversion system, where Rs: ring radii and κs: coupling coefficients.

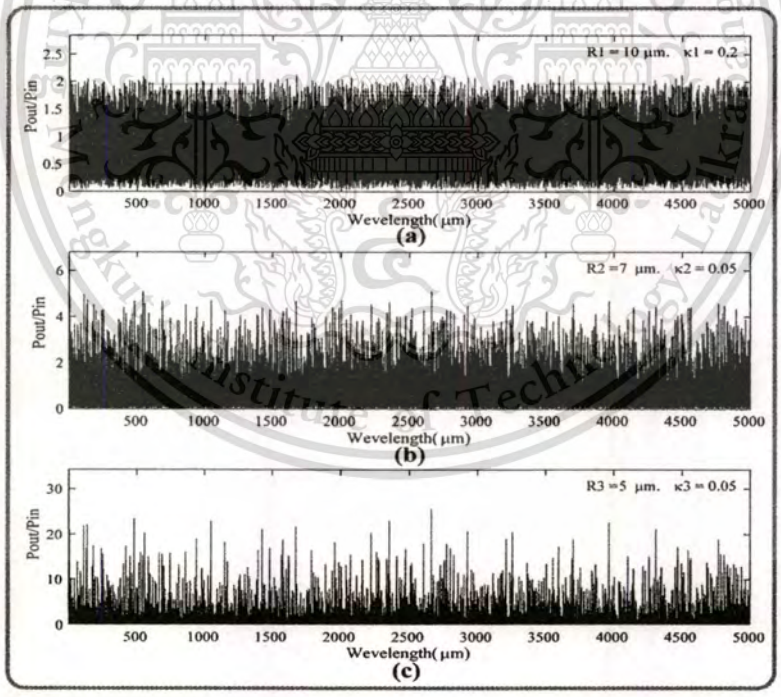

Figure 5.17: Results obtained when a soliton pulse is input into a micro ring resonator system for within NRR.

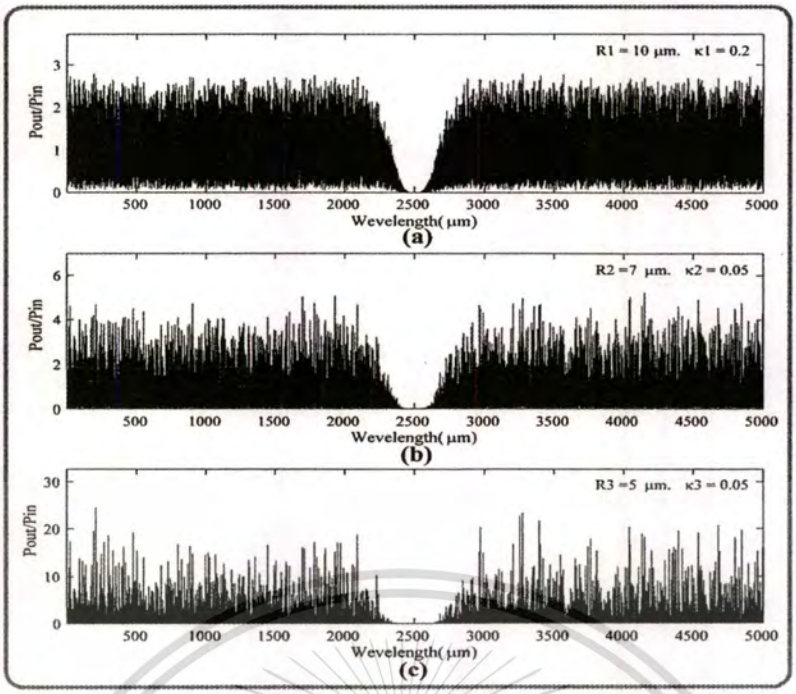

Figure 5.18: Results obtained when a soliton pulse is input into a micro ring resonator system for within NRR.

5.5 Conclusion

In this chapter, the generalized optical filter where the signals in three domains i.e. frequency, wavelength, time can be performed within a single system. The optical communication capacity can be increased by the multi-soliton communication, where more soliton channels can be generated by using the micro ring system. The propagating dark soliton in the optical media can be converted to be a bright soliton by using the ring resonator system incorporating the add/drop multiplexer. By using the reasonable dark soliton input power, the output bright soliton power.

CHAPTER 6
CONCLUSION AND SUGGESTION

6.1 General conclusion

The generalized optical filter where the signals in three domains i.e. frequency, wavelength, time can be performed within a single system. The first interesting result is that the simultaneous fast and slow light could be generated and filtered by using the nonlinear micro ring devices. The system is consisted by a series of four nonlinear micro ring devices. We have shown that the two different frequency bands could be generated and selected, which they are normally used in the up-down-link converters in optical wireless link system. The key advantages of the system are the simultaneous generation of up and down link frequency bands, and the frequency band generation can be formed in the single system. The optical power in the system is generated by using a soliton pulse within the nonlinear Kerr type micro ring devices. Therefore, the remaining optical power is able to perform the link. Further, there are more frequency bands available, which is suitable to implement more applications. Furthermore, we have shown that the broad spectrum of wavelength can be generated and filtered which is capable for high density wavelength multiplexing, where the fast light generation and filtering by using the similar concept is also available. The optical communication capacity can be increased by the multi-soliton communication, where more soliton channels can be generated by using the micro ring system. The required channels are obtained by filtering the large bandwidth signals using the add/drop multiplexer, which is formed by using the micro ring device. Results obtained have shown that the channel spacing (FSR) of 600 pm is achieved. Furthermore, the localized soliton pulses can be stored within the micro ring device, which is available for DWDM based soliton communication. The propagating dark soliton in the optical media can be converted to be a bright soliton by using the ring resonator system incorporating the add/drop multiplexer. By using the reasonable dark soliton input power, the output bright soliton power obtained can be used to perform the common soliton for long distance link, for instance, the output power of bright solitons of 0.5 and 40 W are obtained as shown in Figs. (3) and (4), respectively. The advantage is that the detection of the dark soliton along the through port (transmission line) is difficult, while the detection of the bright one (by the specific user) can be performed by the standard form. This means the use of dark soliton to form the signal security or communication security is plausible, which is also available for network security application. The dark-bright signal amplification is also allowed to use in long distance communication link with security applications.

REFERENCES

[1] Govind P.Agrawal, "Fiber-optic communication systems", Third edition, 2002

[2] D. Anderson. "Optical filters fill many roles." WDM Solutions, June 2001. pp. 97-99

[3] S. Kempainen. "Optical networking lightens carrier-backbone burden." EDN, www.ednmag.com, vol. 8, October 1998. pp. 63-72

[4] E. Pawlowski et al.. "Fabrication of a multichannel Wavelength-division multiplexing-passive optical net demultiplexer with arrayed-waveguide gratings and diffractive optical elements." Appl. Optics, vol. 38, no. 14, 1998. pp. 3039-3045

[5] V. E. Zakharov and A. B. Shabat, "Exact theory of two-dimensional self-focusing and one-dimensional self-modulation of waves in nonlinear media," Zh. Eksp. Teor. Fiz., vol. 61, no. 1, pp. 118–134, 1971.

[6] V. E. Zakharov and A. B. Shabat, "Exact theory of two-dimensional self-focusing and one-dimensional self-modulation of waves in nonlinear media," Sov. Phys. JETP, vol. 34, no. 1, pp. 62–69, 1972.

[7] Steve Blair, "Optical soliton based logic gates", PhD Thesis, University of Coloradoat Boulder, 1998.
download:http://www.ece.utah.edu/~blair/P/dissert.pdf

[8] Singh, S. P. and N. Singh, "Nonlinear effects in optical fibers: Origin, management and applications," Progress In Electromagnetics Research, PIER 73, 249–275, 2007.

[9] Agrawal, G. P., Fiber Optic Communication Systems, 2nd edition, Wiley, New York, 1997.

[10] Singh, S. P. and N. Singh, "Nonlinear effects in optical fibers: Origin, management and applications," Progress In Electromagnetics Research, PIER 73, 249–275, 2007.

[11] Yang, Y., C. Lou, H. Zhou, J. Wang, and Y. Gao, "Simple pulse compression scheme based on filtering self-phase modulationbroadened spectrum and its application in an optical time-division multiplexing systems," Appl. Opt., Vol. 45, 7524–7528, 2006.

[12] Singh, S. P. and N. Singh, "Nonlinear effects in optical fibers: Origin, management and applications," Progress In Electromagnetics Research, PIER 73, 249–275, 2007.

[13] Xiao, X. S., S. M. Gao, Y. Tian, and C. X. Yang, "Optimization of the net residual dispersion for self- phase modulation-impaired systems by perturbation theory," J. lightwave. Tech., Vol. 25, No. 3, 929–937, 2007.

REFERENCES (CONTINUED)

[14] Xiao, X. S., S. M. Gao, Y. Tian, and C. X. Yang, "Analytical optimization of net residual dispersion in SPM-limited dispersionmanaged systems," J. Lightwave. Tech., Vol. 24, No. 5, 2038–2044, 2006.

[15] H. Hasegawa and Y. Kodama, Solitons in Optical Communications (Oxford University Press, New York, 1995).

[16] S. A. Akhmanov, R. V. Khokhlov, and A. P. Sukhorukov, in *Laser Handbook*,Vol. 2, F. T. Arecchi and E. O. Schulz-Dubois, Eds. (North-Holland, Amsterdam, 1972), Chap. E3.

[17] J. I. Gersten, R. R. Alfano, and M. Belic, *Phys. Rev. A* **21**, 1222 (1980).

[18] A. R. Chraplyvy and J. Stone, *Electron. Lett.* **20**, 996 (1984).

[19] R. R. Alfano, Q. X. Li, T. Jimbo, J. T. Manassah, and P. P. Ho, *Opt. Lett.* **14**, 626 (1986).

[20] V. E. Zakharov and A. B. Shabat, *Sov. Phys. JETP* **37**, 823 (1973).

[21] Y. S. Kivshar and B. Luther-Davies, *Phys. Rep.* **298**, 81 (1998).

[22] W. Zhao and E. Bourkoff, *Opt. Lett.* **14**, 703 (1989); *Opt. Lett.* **14**, 808 (1989).

[23] W. J. Tomlinson, R. J. Hawkins, A. M. Weiner, J. P. Heritage, and R. N. Thurston, *J. Opt. Soc. Am. B* **6**, 329 (1989).

[24] P. Emplit, J. P. Hamaide, F. Reynaud, C. Froehly, and A. Barthelemy, *Opt. Commun.* **62**, 374 (1987).

[25] D. Kr¨okel, N. J. Halas, G. Giuliani, and D. Grischkowsky, *Phys. Rev. Lett.* **60**,29 (1988).

[26] A. M. Weiner, J. P. Heritage, R. J. Hawkins, R. N. Thurston, E. M. Krischner, D. E. Leaird, and W. J. Tomlinson, *Phys. Rev. Lett.* **61**, 2445 (1988).

[27] P. Emplit, M. Haelterman, and J. P. Hamaide, *Opt. Lett.* **18**, 1047 (1993).

[28] W. Zhao and E. Bourkoff, *Opt. Lett.* **15** , 405 (1990); *J. Opt. Soc. Am. B* **9**, 1134 (1992).

[29] J. E. Rothenberg and H. K. Heinrich, *Opt. Lett.* **17**, 261 (1992).

[30] D. J. Richardson, R. P. Chamberlain, L. Dong, and D. N. Payne, *Electron. Lett.***30**, 1326 (1994).

[31] O. G. Okhotnikov and F. M. Araujo, *Electron. Lett.* **31**, 2187 (1995).

[32] A. K. Atieh, P. Myslinski, J. Chrostowski, and P. Galko, *Opt. Commun.* **133**, 541 (1997).

[33] M. Nakazawa and K. Suzuki, *Electron. Lett.* **31**, 1084 (1995).

[34] M. Nakazawa and K. Suzuki, *Electron. Lett.* **31**, 1076 (1995).

REFERENCES (CONTINUED)

[35] P. Emplit, M. Haelterman, R. Kashyap, and M. DeLathouwer, *IEEE Photon. Technol. Lett.* **9**, 1122 (1997).

[36] R. Leners, P. Emplit, D. Foursa, M. Haelterman, and R. Kashyap, *J. Opt. Soc. Am. B* **14**, 2339 (1997).

[37] R. Leners, P. Emplit, D. Foursa, M. Haelterman, and R. Kashyap, J. Opt. Soc. Am. B 14, 2339 (1997).

[38] P.P. Yupapin and N. Pornuwancharoen, "Guided Wave Optics and Photonics: Micro Ring Resonator Design for Telephone Network Security," Nova Science Publishers, New York, 2008.

[39] P.P. Yupapin and W. Suwancharoen, "A Novel Technology for Mobile Telephone Networks and Security," Mobile Telephones: Networks, Applications, and Performance, Editors : Alvin C. Harper and Raymond V. Buress, Nova Science Publishers, New York, (2008)265-274.

[40] P.P. Yupapin and S. Suchat, "Mobile Telephone Network Security via Nonlinear Integrated Optic Devices," Engineering Transaction, MUT, June 2008.

[41] S. Mitatha, K. Dejhan, P.P. Yupapin and N. Pornsuwancharoen, "Chaotic Signal Generation and Coding using a Nonlinear Micro Ring Resonator," International Journal of Light and Electron Optics, 2008. DOI: 10.1016/j.ijleo.2008.05.028.

[42] S. Mitatha, K. Dejhan, P.P. Yupapin and N. Pornsuwancharoen, "High Capacity and Security Packet Switching using the Nonlinear Effects in Micro Ring Resonators," International Journal of Light and Electron Optics, 2008. DOI: 10.1016/j.ijleo.2008.05.032.

[43] S. Chaiyasoonthorn, S. Mitatha, K. Dejhan and P.P. Yupapin, "Attosecond Pulse and Its Beyond Generation Based on Multi-stage Micro Ring Resonators," J. Adv. Mater. Res., 2008. [Article in press]

[44] M. T. Zhou, J.D. Zhang, A.B. Sharma, Y. Zhang, S. Xiao, M. Fujise, "Design of Millimeter-wave Fiber-wireless Downlink with Remote Local-oscillator Delivery by using Dual-electrode Mach-Żehnder Modulators Configured for Optical Single-sideband Modulation," Opt. Commun., 269(2007)69-75.

[45] M. T. Zhou, Q.J. Wang, B. Luo, Y.X. Guo, L.C. Ong, Y. Zhang, Y.C. Soh, R. Miura, "Performance Improvement and Wavelength Reuse in Millimeter-wave Radio-over-fiber Links Incorporating All-fiber Optical Interleaver," Opt. Commun., 281(2008)2572-2581.

[46] Y. Kokubun, Y. Hatakeyama, M. Ogata, S. Suzuki, and N. Zaizen, "Fabrication Technologies for Vertically Coupled Microring Resonator with Multilevel Crossing Busline and Ultracompact-Ring Radius," IEEE J. of Selected Topics in Quantum Electronics, 11(2005)4-10.

REFERENCES (CONTINUED)

[47] LUMICS Devices for Optical Systems, Laser Diodes and Fiber Laser, Product Catalog 2007. [www.lumics.com]

[48] C. Taepanich and P.P.Yupapin, Optical Soliton Equation and Its Application in Optical Devices Design For High Speed Communication, NECTEC TECHNICAL JOURNAL, 11(2000)143.

[49] P.P. Yupapin, N. Pornsuwancharoen and J. Ali, Optical Soliton in Micro Ring Resonators: Unexpected Results and Applications, Nova Science Publishers, New York, 2008.

[50] P.P. Yupapin, N. Pornsuwanchroen and S. Chaiyasoonthorn, "Attosecond pulse generation using nonlinear micro ring resonators," Microw. and Opt. Technol. Lett., 50(12), 2008.

[51] C. Fietz and G. Shvets, "Nonlinear polarization conversion using micro ring resonators", Opt. Lett., 32(2007)1683.

[52] Y. Kokubun, Y. Hatakeyama, M. Ogata, S. Suzuki, and N. Zaizen, "Fabrication technologies for vertically coupled micro ring resonator with multilevel crossing busline and ultracompact-ring radius," IEEE J. of Selected Topics in Quantum Electron., 11(2005)4.

[53] Y. Su, F. Liu and Q. Li, "System performance of show-light buffering and storage in silicon nano-waveguide," Proc. SPIE, 6783(2007)67832P.

[54] Mário F. S. Ferreira, "Nonlinear Effects in Optical Fibers: Limitations and Benefits," Proc. SPIE, 6793, 02(2007).

[55] P.P. Yupapin, W. Suwanchareon and S. Suchat, "Nonlinearity Penalties and Benefits of Light Traveling in a Fiber Optic Ring Resonator," Int. J. of Light and Electron Opt., 2007. DOI : 10.1016/j.ijleo.2007.07.009.9Available online).

[56] P.P. Yupapin and N. Pornsuwancharoen, Guided Wave Optics and Photonics: Micro Ring Resonator Design for Telephone Network Security, Nova Science Publishers, New York, 2008.

[57] P.P. Yupapin and P. Saeung, Photonics and Nanotechnology, World Scientific, Singapore, 2008.

[58] Y. Su, F. Liu and Q. Li, "System Performance of Slow-light Buffering and Storage in Silicon Nano-waveguide," Proc. SPIE, 6783, 68732P(2007).

[59] P.P. Yupapin, N. Pornsuwanchroen and S. Chaiyasoonthorn, "Attosecond Pulse Generation using Nonlinear Micro Ring Resonators," Microw. and Opt. Technol. Lett., 50, 3108(2008).

[60] Y. S. Kivshar and B. Luther-Davies, "Dark Optical Solitons: Physics and applications," Phys. Rep., 298, 81(1998).

[61] W. Zhao and E. Bourkoff, "Propagation properties of Dark Solitons," Opt. Lett., 14, 703(1989).

REFERENCES (CONTINUED)

[62] I.V. Barashenkov, "Stability Criterion for Dark Soliton," Phys. Rev. Lett., 77, 1193(1996).

[63] D. N. Christodoulides, T. H. Coskun, M. Mitchell, Z. Chen and M. Segev, "Theory of Incoherent Dark Solitons," Phys. Rev. Lett., 80, 5113(1998).

[64] A. D. Kim, W. L. Kath and C. G. Goedde, "Stabilizing Dark Solitons by Periodic Phase-Sensitive Amplification," Opt. Lett., 21, 465(1996).

[65] B. A. Malomed, A. Mostofi and P. L. Chu, "Transformation of a Dark Soliton into a Bright Pulse," J. Opt. Soc. Am. B, 17, 507(2000).

[66] P.P. Yupapin and W. Suwancharoen, "Chaotic Signal Generation and Cancellation using a Micro Ring Resonator incorporating an Optical Add/drop Multiplexer, Opt. Commun., 280, 343(2007).

APPENDIX

List of Publication

[1] P.P. Yupapin, N Sangwara and N. Pornsuwancharoen, **Generalized Optical Filters using a Nonlinear Micro Ring Resonator System**, International Journal of Light and Electron Optic,2009 (Impact Factor 2008: 0.507)

[2] N. Pornsuwancharoen, P. Youplao, N. Sangwara, P.P. Yupapin, **Multi-wavelength Generation of an Extreme-narrow Pulse using a Ring Resonator System for Bio-cells Microscopy**, International Journal of Light and Electron Optic,2009 (Impact Factor 2008: 0.507)

[3] N. Sangwara, N. Pornsuwancharoen and P.P. Yupapin, **Soliton Pulses Generation and Filtering using Micro Ring Resonators for DWDM Based Soliton Communication,** International Journal of Light and Electron Optic,2009 (Impact Factor 2008: 0.507)

[4] N. Pornsuwancharoen, N. Sangwara and P.P. Yupapin, **Generalized Fast and Slow Lights using Multi-state Micro Ring Resonators for Optical Wireless Links**, International Journal of Light and Electron Optic,2009 (Impact Factor 2008: 0.507)

[5] K. Sarapat,N. Sangwara, K. Srinuanjan and P.P. Yupapin, **A Novel Dark-Bright Optical Solitons Conversion System and Power Amplification,** Optical Engineering, Vol.48(4), 2009, pp.045004. (Impact Factor 2008: 0.722)

AUTHOR BIOGRAPHY

Author	Narong Sangwara
Date of Birth	August 5, 1981
Place of Birth	Phetchaboon, Thailand
E-mail	narong_5@hotmail.com
Bachelor Degree	B.Sc(Physics)
Institution	Thepsatri Rajabhat University, Thailand
Year of Graduation	2003
Master Degree	M.Sc(Applied Physics)
Institution	King Mongkut's Institute of Technology Landkrabang, Thailand
Year of Graduation	2006
Contact Address	Department of Physics, Faculty of Science and Technology, Rajamangala University of Technology Krungthep, Bangkok 10120, Thailand